Title
Influence of water on clumped-isotope bond reordering kinetics in calcite

Authors
Brenner, Dana C
Passey, Benjamin H
Stolper, Daniel A

Publication Date
2018-03-01

DOI
10.1016/j.gca.2017.12.026

Peer reviewed

Influence of water on clumped-isotope bond reordering kinetics in calcite

Author links open overlay panel Dana C. Brenner[a] Benjamin H. Passey[a1] Daniel A. Stolper[b]
Show more

https://doi.org/10.1016/j.gca.2017.12.026

Abstract

Oxygen self-diffusion in calcite and many other minerals is considerably faster under wet conditions relative to dry conditions. Here we investigate whether this “water effect” also holds true for solid-state isotope exchange reactions that alter the abundance of carbonate groups with multiple rare isotopes (‘clumped’ isotope groups) via the process of solid-state bond reordering. We present clumped-isotope reordering rates for optical calcite heated under wet, high-pressure (100 MPa) conditions. We observe only modest increases in reordering rates under such conditions compared with rates for the same material reacted in dry CO_2 under low-pressure conditions. Activation energies under wet, high-pressure conditions are indistinguishable from those for dry, low-pressure conditions, while rate constants are resolvably higher (up to ∼3 times) for wet, high-pressure relative to dry, low-pressure conditions in most of our interpretations of experimental results. This contrasts with the water effect for oxygen self-diffusion in calcite, which is associated with lower activation energies, and diffusion coefficients that are ≥10^3 times higher compared with dry (pure CO_2) conditions in the temperature range of this study (385–450 °C). The water effect for clumped-isotopes leads to calculated apparent equilibrium temperatures (“blocking temperatures”) for typical geological cooling rates that are only a few degrees higher than those for dry conditions, while O self-diffusion blocking temperatures in calcite grains are ∼150–200 °C lower in wet conditions compared with dry conditions. Since clumped-isotope reordering is a distributed process that occurs throughout the mineral volume, our clumped-isotope results support the suggestion of Labotka et al. (2011) that the water effect in calcite does not involve major changes in bulk (volume) diffusivity, but rather is primarily a surface phenomenon that facilitates oxygen exchange between the calcite surface and external fluids. We explore the mechanism(s) by which clumped isotope reordering rates may be modestly increased under wet, high-pressure conditions, including changes in defect concentrations in the near surface environment due to reactions at the water–mineral interface, and lattice deformation resulting from pressurization of samples.

- **Previous** article in issue
- **Next** article in issue

Keywords

Clumped-isotopes
Calcite
Water
Solid-state diffusion
Reordering kinetics

1. Introduction

The presence of water can affect the chemical reactions and rates of those reactions that occur in a variety of geological systems including in igneous, metamorphic, and sedimentary systems. Water appears to significantly change (by orders of magnitude) reaction rates and pathways during solid-state diffusion both between and within minerals (Kronenberg et al., 1984, Hochella and White, 1990a, Farver, 1994, Labotka et al., 2000, Behrens and Zhang, 2001, Wang et al., 2004, Hier-Majumder et al., 2005; Brown et al., 1999, Brown, 2001). For example, the presence of water enhances, by a factor of 10–50, Fe–Mg interdiffusion in olivine (Wang et al., 2004, Hier-Majumder et al., 2005), Ar diffusion in rhyolitic and albitic melts (Behrens and Zhang, 2001), and the diffusivity of oxygen in carbonate minerals (Kronenberg et al., 1984, Farver, 1994, Labotka et al., 2000, Labotka et al., 2011). Here we focus on how water affects isotope-exchange rates between carbonate groups within calcite as studied in the laboratory using the distribution of multiply isotopically substituted carbonate molecules (commonly referred to as “clumped” isotopes).

Within the past decade, carbonate clumped-isotope thermometry has emerged as an important tool for answering for geologic questions ranging from the temperature evolution of Earth’s oceans over the Phanerozoic (*e.g.*, Ghosh et al., 2006a, Came et al., 2007, Bernasconi et al., 2011, Eiler, 2011, Finnegan et al., 2011, Dennis et al., 2013, Grauel et al., 2013, Cummins et al., 2014, Drury and John, 2016), Cenozoic uplift history of Earth’s major mountain ranges (Ghosh et al., 2006b, Huntington et al., 2010, Huntington et al., 2014, Quade et al., 2011, Leier et al., 2013, Huntington and Lechler, 2015; Kar et al., 2016), sedimentary basin burial histories pertinent to fossil fuel exploration (Dale et al., 2014, Henkes et al., 2014, Shenton et al., 2015), and low-temperature (<400 °C) metamorphism (Ferry et al., 2011, Lloyd et al., 2017). The carbonate clumped-isotope thermometer is based on the temperature-dependence of

isotope-exchange reactions between carbonate groups with two or more rare, heavy isotopes (clumped isotopologues) in chemically equilibrated systems. In calcium carbonate minerals, the predominant clumped isotopologue exchange reaction is:

(1) $Ca^{13}C^{18}O^{16}O_2 + Ca^{12}C^{16}O_3 \leftrightarrow Ca^{13}C^{16}O_3 + Ca^{12}C^{18}O^{16}O_2$

For an isotopically equilibrated system, the abundance of multiply substituted carbonate isotopologues relative to a random isotopic distribution is a monotonic function of temperature (Schauble et al., 2006, Ghosh et al., 2006a). At low temperature, clumped isotopologue abundances are more enriched relative to a random distribution for an isotopically equilibrated system than at high temperature (Schauble et al., 2006, Ghosh et al., 2006a). This temperature dependence provides the basis for carbonate clumped-isotope geothermometry (Schauble et al., 2006, Ghosh et al., 2006a).

Carbonates that precipitate in internal isotopic equilibrium will have a clumped-isotope signature that reflects the minerals' formation temperatures. Non-equilibrium clumped-isotope distributions can also occur in nature. For example, growth of carbonate minerals at fast rates prevents CO_3^{2-} groups from maintaining isotopic equilibrium with water (and thus internal isotopic equilibrium between carbonate groups) and can result in non-equilibrium clumped isotope abundances (*e.g.*, Affek et al., 2008, Daëron et al., 2011, Saenger et al., 2012, Kluge et al., 2014, Affek and Zaarur, 2014, Tripati et al., 2015). These processes all involve isotope-exchange reactions between carbonate and water.

Isotope-exchange processes also occur in minerals such as when C–O bonds are broken and remade within the mineral lattice, resulting in the exchange of oxygen atoms between differing carbonate ion groups (Henkes et al., 2014, Ghosh et al., 2006a, Dennis and Schrag, 2010, Eiler, 2011, Stolper and Eiler, 2015, Passey and Henkes, 2012). Such solid-state isotope-exchange processes can alter the clumped-isotope compositions of carbonate minerals in a variety of scenarios including burial (Henkes et al., 2014, Shenton et al., 2015), exhumation (Ghosh et al., 2006b, Huntington et al., 2010, Huntington and Lechler, 2015), and contact and regional metamorphism (Ferry et al., 2011, Lloyd et al., 2017). We use the term 'reordering' for these solid-state isotopic exchange reactions that occur within the calcite crystal lattice in response to a thermal perturbation. Reordering refers to the change in the degree of internal isotopic order for C–O bonding of the mineral when it is out of thermodynamic equilibrium. Order relates to the abundance of clumped isotopologue groups—calcite formed in isotopic equilibrium at a lower versus higher temperature has a higher concentration of clumped isotopologue groups relative to that expected for a random distribution of isotopes amongst all isotopologue groups and is thus more

ordered than the calcite formed at higher temperature. Some potential factors that may influence the rates of these reordering reactions include the mineral type (Ferry et al., 2011, Lloyd et al., 2017, Ryb et al., 2017), minor element substitution in the mineral lattice (Kronenberg et al., 1984), water fugacity (Kronenberg et al., 1984, Farver, 1994, Labotka et al., 2011), pressure (Labotka et al., 2000, Labotka et al., 2004), the pH and dissolved ion composition of fluid in contact with the mineral (Hill et al., 2014, Tripati et al., 2015), and deformation (Siman-tov et al., 2016, Ryb et al., 2017). Understanding the importance of these various factors to reordering kinetics is necessary to evaluate and use carbonate clumped-isotope measurements in systems where reordering reactions have occurred.

The temperature dependence of clumped-isotope reordering kinetics in calcite has been studied in detail under dry (low fH_2O) conditions (Passey and Henkes, 2012, Henkes et al., 2014; Stolper and Eiler, 2015). However, the other factors discussed above have not been thoroughly investigated, except for a study of the effect of mineralogy(clumped-isotope reordering in the carbonate component of apatitemineral; Stolper and Eiler, 2015) and limited experiments on the influence of water (Passey and Henkes, 2012). Most shallow crustal processes, including burial diagenesis and contact metamorphism, occur in the presence of water and under elevated pressures (Ferry and Dipple, 1991, Beckert et al., 2016). Therefore, it is important to understand how the presence of water influences the kinetics of clumped-isotope reordering.

It is well known, based on tracer diffusion studies, that solid-state oxygen diffusivities differ in wet versus dry conditions (Kronenberg et al., 1984, Farver, 1994, Labotka et al., 2011). These tracer diffusion studies evaluate diffusivities in the near-surface (outer few micrometers) of the sample as, on laboratory timescales, tracers only diffuse a relatively short distance into the sample (typically ≤2 μm) (Kronenberg et al., 1984, Farver, 1994, Labotka et al., 2000, Labotka et al., 2004, Labotka et al., 2011). The diffusivities obtained in these studies are generally assumed to be applicable to diffusivities that occur in the bulk mineral volume, far from the surface. As clumped carbonate ions are distributed throughout the bulk mineral, changes in their abundance due to bond reordering should reflect processes that occur throughout the mineral lattice, as opposed to solely on the surface.

Here we study experimentally how wet, high-pressure (wet-HP) conditions influence calcite clumped-isotope reordering kinetics. Passey and Henkes (2012) conducted a preliminary set of wet-HP reactions (100 MPa) at a single reaction temperature (420–422 °C) and observed no resolvable difference in reordering rate relative to reactions performed on the same mineral sample, a spar calcite (NE-CC-1), reacted under dry

conditions at 425 °C. They also presented two data points for samples reacted under relatively low-pressure (0.1 MPa) wet conditions at 475 °C, which again showed little difference from samples reacted under dry conditions. Here we describe a larger set of laboratory experiments where an optical calcite (material MBG-CC-1) was heated under wet conditions at elevated pressures (100 MPa) to simulate aqueous, high-pressure natural conditions. We compare the resulting changes in clumped-isotope compositions to analogous results for the same calcite heated under dry, low-pressure (dry-LP) conditions using data from Passey and Henkes (2012). We evaluate our results in terms of the bond reordering models of Passey and Henkes (2012) and Stolper and Eiler (2015). We then examine the influence of wet-HP conditions on clumped isotope alteration owing to heating and cooling over geologic timescales. Finally, we discuss some implications of our results for understanding the so-called water effect, that is, the enhanced O diffusivity associated with the presence of water.

2. Methods

All experiments were performed on aliquots of sample MGB-CC-1, an optical calcite from Minas Gerais, Brazil (Wards Scientific Co.). This is the same optical calcite used in Passey and Henkes (2012) to study dry-LP (0.1 MPa) clumped-isotope bond reordering kinetics. Calcite crystals were first passed through a 0.250–0.125 mm mesh. Aliquots of granular calcite (~35 mg) and deionized water (25–75 mg; *i.e.*, sufficient quantity to maintain hydrostatic equilibrium at reaction pressures) were sealed in silver capsules (3.04 mm I.D., 0.23 mm wall thickness, 3.5 mm O.D., 1 cm length). We note that in these experiments, water is not expected to be consumed appreciably by reaction with calcite. As such, any variability in the H_2O/calcite ratio among different capsules should have little influence on experimental results. The capsules were welded shut with a H_2 + O_2 torch, and heating of the contents during welding was minimized by tightly wrapping each capsule with wet strips of paper tissue. We assumed the deionized water had a $\delta^{18}O_{water}$ value close to −6‰, VSMOW, based on Baltimore tap water $\delta^{18}O_{water}$ values as reported by Li et al. (2015). The sealed capsules were weighed, heated in an oven (~120 °C) for 2 h, and re-weighed to check for leaks. The capsules were heated in 14.3 mm outside diameter by 4.8 mm interior diameter (=9/16″ O.D. by 3/16″ I.D.) stainless steel reactors (High Pressure Equipment Company). Capsules were placed in individual reactor lines and brought to 100 MPa under hydraulic pressure (with water as the pressurizing medium). We selected 100 MPa pressure to simulate shallow crustal burial (~10 km) and to compare our results directly with the oxygen diffusion studies of Farver (1994) and Labotka et al. (2000) that were conducted at 100 MPa.

Pressure was maintained to within ∼3 MPa for the duration of heating. Insulated coaxial heater assemblies consisting of high watt density band heaters (7.6 cm wide, 3.8 cm diameter) wrapped around 12.7 cm long, 3.8 cm diameter copper blocks were brought to temperature away from the capsule-containing part of the reactor, and then moved into place over the capsule area in order to bring the capsules to temperature quickly, approaching within 5 °C of the experimental temperature in 14 ± 7 min.
Temperatures were measured with K-type thermocouples terminating inside the high-pressure environment, directly alongside the sample capsules. There are two sources of uncertainty in the temperature of sample capsules during reaction: Uncertainty in the calibration of the thermocouples, and uncertainty due to temperature gradients along the lengths of the coaxial heaters. We calibrated our thermocouples against the melting point of Zn prior to use, and on this basis conservatively estimate a temperature uncertainty of ±2 °C in the temperature range of our experiments (375–450 °C). The temperature gradient in the hot spot at the center of the heaters was measured to be approximately 2 °C/cm displacement from the center of the heater. The positional uncertainty among the hot-spot of the heater, capsule, and internal thermocouple was ∼1.5 cm, translating to a temperature range of 3 °C (that is, ±1.5 °C) due to the temperature gradient. Thus, the overall root sum of squares temperature uncertainty is ±2.5 °C. During heat-up, the pressurizing pump was adjusted as necessary in order to maintain a pressure of 100 ± 3 MPa.
Samples remained at temperatures of 385–450 °C for time periods of 60 min to 4 days. Upon completion of each experiment, the band heaters were removed from the sample-containing part of the reactor, and the reactors were rapidly quenched with a compressed air gun to temperatures below 80 °C in less than 120 s, in an effort to minimize any reordering during cooling. The pressurizing pump was adjusted as necessary to maintain a pressure of 100 ± 3 MPa during cooling. Once cooled, samples were weighed, placed in an oven (∼60 °C) for 2 h, and reweighed to check for leaks. Any compromised samples were discarded. The cooler oven temperature in this step (60 °C) relative to the initial leak-check step (120 °C) is simply a consequence of equipment availability at the time of the experiments. The difference in temperature is not expected to impact our results, as both temperatures are sufficiently high to drive evaporative loss from sample capsules (if they are not leak-tight), and both temperatures are too low for solid-state clumped isotope reordering. Finally, the capsules were opened, excess water was wicked away with tissue paper, and the calcite samples were dried in an oven (∼120 °C) for 3 h.

Sample isotopic compositions including Δ_{47} values were measured at Johns Hopkins University using an automated preparation device (Passey et al., 2010) coupled to a Thermo MAT 253 mass spectrometer. Briefly, samples were reacted in a common acid bath (100% H_3PO_4, 90 °C), and the evolved CO_2 was purified by passage through multiple −78 °C cryogenic traps, an Ag-wool getter, and a −20 °C gas chromatography column (Poropak), prior to admittanceinto the mass spectrometer. Isotopic bond reordering was monitored using the parameter Δ_{47}, which is defined as:

(2)Δ47=R47R∗47-1-R46R∗46-1-R45R∗45-1×1000

where R^{*i} is the abundance ratio of the heavy isotopologue of mass *i*divided by the common isotopologue (mass 44), and the asterisk denotes a random distribution of isotopes among all isotopologues (Affek and Eiler, 2006). Raw Δ_{47} values (sample gas measured against a reference gas standard consisting of 6 acquisitions of 9 cycles per acquisition with a 26 s counting period per gas per cycling for a total of 1404 s) were calculated assuming the RPDB13, RVSMOW18, RVSMOW17, triple oxygen isotope slope λ of Gonfiantini et al. (1995), as described by Huntington et al. (2009), and then normalized relative to heated gases (CO_2 heated to 1000 °C) and equilibrated gases (CO_2equilibrated with water at 30 °C) using the absolute reference frame (ARF) approach described by Dennis et al. (2011). These same parameters were used in data processing for the dry, low-pressure experiments on MGB-CC-1 calcite (Passey and Henkes, 2012). Thus the Δ_{47} values presented here are directly comparable to the values given by Passey and Henkes (2012), and for the purposes of this study there is no need to reprocess data using other parameters related to ^{17}O (*e.g.*, Daëron et al., 2016, Schauer et al., 2016). When necessary, a Matlab code was used to model temporal drift in the heated and equilibrated gas reference lines. To evaluate instrument precision and stability, we routinely analyzed a low temperature internal carbonate standard (102-GC-AZ01), and two high temperature marbles, international standard NBS-19 and internal standard HAF-Carrara (the latter provided by Hagit Affek, and also known as YCM – Yale Carrara Marble) (Table 1). All Δ_{47} values are reported as 25 °C acid digestion-equivalent values using the 90 °C versus 25 °C correction of 0.0823‰ recommended by Defliese et al. (2015) (Table 1). The Δ_{47} data for dry reordering experiments reported in Passey and Henkes (2012) were corrected using an acid temperature correction of 0.081‰, and hence we add a constant value of 0.0013‰ to those data, for purposes of comparison with the results presented here.

Table 1. Results for optical calcite heating experiments reacted under wet, high-pressure conditions (P = 100 MPa).

Sample ID	T (°C)	Time (minutes)	$\delta^{18}O$[*] (VPDB)	$\delta^{13}C$[*] (VPDB)	Δ_{47}[†,‡] (ARF)	Corrected Δ_{47}[†,§] (ARF)
Unreacted (n = 4)		–	−9.49 ± 0.13	−4.71 ± 0.02	0.631 ± 0.012	–
DBRX-053	385	60	−9.55	−4.70	0.593 ± 0.012	0.594
DBRX-046	385	240	−9.61	−4.71	0.578 ± 0.008	0.579
DBRX-056	385	960	−9.69	−4.70	0.556 ± 0.010	0.558
DBRX-056	385	960	−9.74	−4.67	0.544 ± 0.007	0.548
DBRX-043	385	1440	−9.94	−4.76	0.538 ± 0.009	0.544
DBRX-043	385	1440	−9.91	−4.70	0.539 ± 0.010	0.544
DBRX-051	385	2882	−9.83 ± 0.02	−4.68	0.506 ± 0.009	0.510
DBRX-051	385	2882	−9.88	−4.73	0.516 ± 0.014	0.521
DBRX-049	385	4320	−9.99	−4.70	0.524 ± 0.002	0.530
DBRX-059	385	5760	−10.09	−4.73	0.518 ± 0.009	0.525
DBRX-059	385	5760	−9.90 ± 0.02	−4.69 ± 0.02	0.491 ± 0.019	0.494
DBRX-035	405	60	−9.58	−4.70	0.565 ± 0.008	0.566
DBRX-039	405	239	−9.65	−4.71	0.546 ± 0.007	0.548
DBRX-055	405	961	−9.82	−4.71	0.513 ± 0.007	0.516
DBRX-040	405	1440	−9.81	−4.71	0.457 ± 0.008	0.459
DBRX-040	405	1440	−9.76	−4.71	0.478 ± 0.012	0.481
DBRX-037	405	2880	−9.79	−4.71	0.464 ± 0.013	0.466
DBRX-037	405	2880	−9.77	−4.72	0.454 ± 0.007	0.457

Sample ID	T (°C)	Time (minutes)	$\delta^{18}O$[*] (VPDB)	$\delta^{13}C$[*] (VPDB)	Δ_{47}[†,‡] (ARF)	Corrected Δ_{47}[†,§] (ARF)
DBRX-048	405	4319	−9.81	−4.67	0.427 ± 0.006	0.429
DBRX-048	405	4319	−10.03	−4.69	0.417 ± 0.007	0.420
DBRX-058	405	5760	−9.99	−4.70	0.404 ± 0.013	0.406
DBRX-027	426	60	−9.59	−4.71	0.534 ± 0.014	0.536
DBRX-034	426	241	−9.64	−4.70	0.511 ± 0.012	0.513
DBRX-054	425	960	−9.84	−4.71	0.461 ± 0.012	0.464
DBRX-054	425	960	−9.80	−4.71	0.469 ± 0.017	0.472
DBRX-028	426	1440	−9.80	−4.70	0.444 ± 0.012	0.446
DBRX-029	426	2880	−10.05	−4.73	0.397 ± 0.009	0.399
DBRX-029	426	2880	−9.94	−4.70	0.371 ± 0.012	0.372
DBRX-057	425	4320	−9.94	−4.69	0.387 ± 0.009	0.389
DBRX-057	425	4320	−9.93	−4.66	0.359 ± 0.010	0.360
DBRX-068	425	5760	−9.92	−4.69	0.349 ± 0.015	0.350
DBRX-052	450	60	−9.63	−4.70	0.488 ± 0.013	0.490
DBRX-045	450	240	−9.73	−4.72	0.433 ± 0.005	0.434
DBRX-042	450	960	−9.90	−4.73	0.363 ± 0.006	0.364
DBRX-042	450	960	−9.69	−4.70	0.349 ± 0.012	0.350
DBRX-044	450	1440	−9.80	−4.71	0.325 ± 0.012	0.325
DBRX-044	450	1440	−9.83	−4.68	0.348 ± 0.008	0.349

Sample ID	T (°C)	Time (minutes)	$\delta^{18}O$* (VPDB)	$\delta^{13}C$* (VPDB)	Δ_{47}†,‡ (ARF)	Corrected Δ_{47}†,§ (ARF)
DBRX-050	450	2880	−9.97	−4.69	0.314 ± 0.007	0.314
DBRX-050	450	2880	−10.03	−4.70	0.319 ± 0.008	0.319
DBRX-061	450	5760	−10.04	−4.70	0.318 ± 0.012	0.318
DBRX-061	450	5760	−9.91	−4.70	0.309 ± 0.008	0.309
Standards						
102-GC-AZ01 (n = 18)			−14.53 ± 0.09	0.531 ± 0.07	0.695 ± 0.014	
NBS-19 (n = 9)			−2.26 ± 0.05	2.04 ± 0.02	0.393 ± 0.011	
HAF-Carrara (n = 10)			−1.87 ± 0.04	2.35 ± 0.02	0.390 ± 0.008	

* Reported uncertainty is the internal precision (1σ) in $\delta^{18}O$ and $\delta^{13}C$ observed across six consecutive analyses (acquisitions). Internal precision is ≤0.01 unless indicated. For standards and unreacted material analyzed multiple times, the reported uncertainty is 1σ for external replicates.

† Values are reported in the absolute reference frame after Dennis et al. (2011).

‡ Reported uncertainty is the internal standard error observed across six consecutive analyses (acquisitions). Standards and unreacted material error is 1σ for external replicates.

§ Values corrected to account for Δ_{47} fraction attributed to reprecipitation in equilibrium with reaction temperature. See text, Section Section 3, for full explanation. The magnitude of correction is less than 0.007‰ in all cases.

SEM imaging was conducted on a FEI Quanta 200 Environmental SEM at the Johns Hopkins University Integrated Imaging Center. Images were taken at 1.50 keV accelerating voltage, 4.0 spot size, and a pressure of 80 Pa. XRD analysis was done on a Philips PANalytical X'Pert X-ray diffractometer at Johns Hopkins University.

3. Results

Stable isotope data are reported in Table 1. The $\delta^{13}C$, $\delta^{18}O$, and Δ_{47} values of experimental products versus reaction time are shown in Fig. 1, Fig. 2, Fig. 3. There was no change in $\delta^{13}C$ (VPDB) within the limits of analytical precision (±0.08‰, 1σ). In contrast, the $\delta^{18}O$ (VSMOW) values for wet-HP reactions decrease progressively with reaction duration by as much as −0.6‰ (Fig. 2). Analytical precision for $\delta^{18}O$ was ±0.09‰ (1σ).

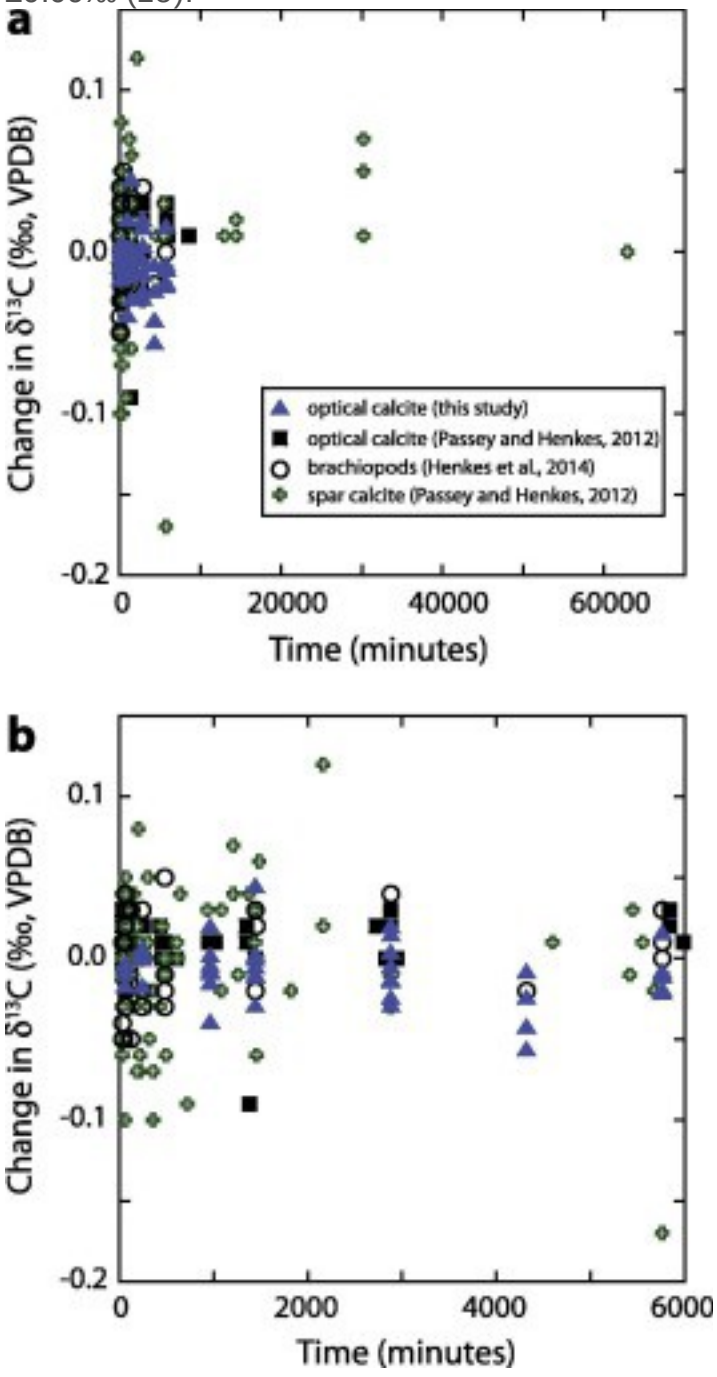

1. Download high-res image (231KB)

2. Download full-size image

Fig. 1. (a) Plot of the change in $\delta^{13}C$ value of reacted samples as a function of reaction time. Symbols represent different experimental studies: blue triangles are wet-HP optical calcite individual measurements from the current study, black squares are dry-LP optical calcite individual measurements from Passey and Henkes (2012), open circles are dry-LP brachiopod replicate averages from Henkes et al. (2014), and green crosses are dry-LP spar calcite individual measurements from Passey and Henkes (2012). Error bars are omitted for clarity; the 1σ precision for repeated analyses of homogenous carbonate standards is better than 0.05‰. (b) Same as (a) but zoomed into shorter reaction times. (For interpretation of the references to colour in this figure legend, the reader is referred to the web version of this article.)

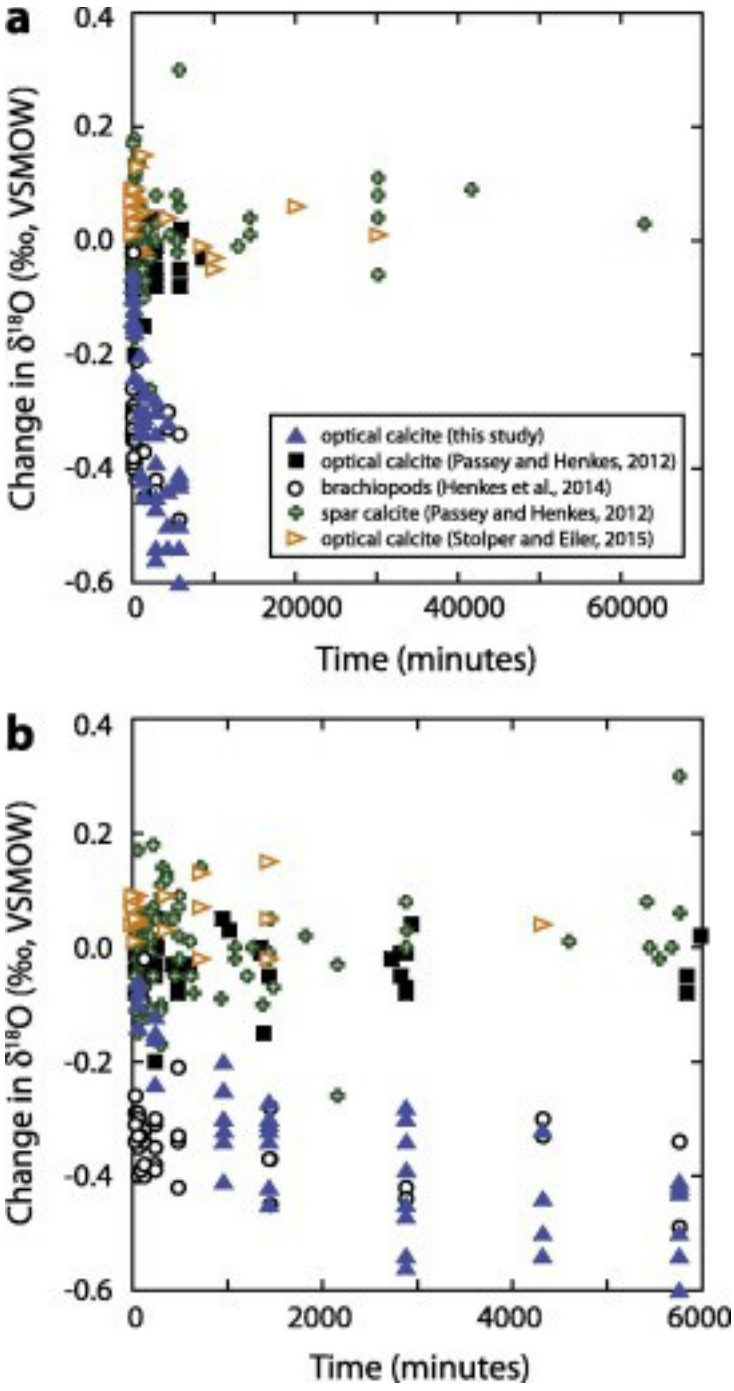

1. Download high-res image (279KB)
2. Download full-size image

Fig. 2. (a) Plot of the change in $\delta^{18}O$ value of reacted samples as a function of reaction time. Symbols represent different experimental studies: blue triangles are wet-HP optical calcite individual measurements from the current study, black squares are dry-LP optical calcite individual measurements from Passey and Henkes (2012), open circles are dry-LP brachiopod replicate averages from Henkes et al. (2014), green crosses are

dry-LP spar calcite individual measurements from Passey and Henkes (2012), and orange triangles are dry, mid-pressure (50–65 MPa) optical calcite replicate averages from Stolper and Eiler (2015). Error bars are omitted for clarity; the 1σ precision for repeated analyses of homogeneous carbonate standards is ∼0.1‰. (b) Same as (a) but zoomed into shorter reaction times. We note that although the brachiopod samples from Henkes et al. (2014) were reacted under nominally dry conditions, small amounts of water condensate were sometimes observed inside of reaction tubes following the heating experiments. (For interpretation of the references to colour in this figure legend, the reader is referred to the web version of this article.)

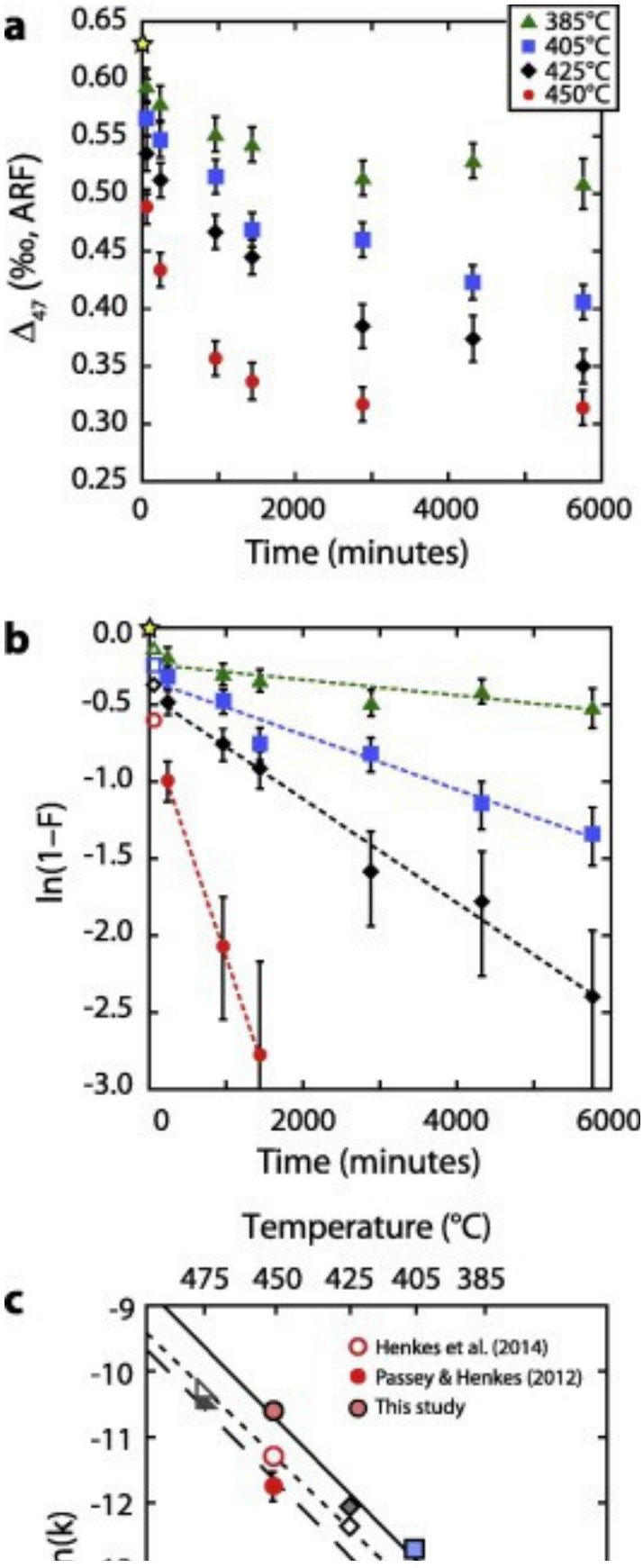
a
0.65
0.60
0.55
0.50
0.45
0.40
0.35
0.30
0.25
Δ_{47} (‰, ARF)
385°C
405°C
425°C
450°C
0
2000
4000
6000
Time (minutes)
b
0.0
-0.5
-1.0
-1.5
-2.0
-2.5
-3.0
ln(1−F)
0
2000
4000
6000
Time (minutes)
Temperature (°C)
475 450 425 405 385
c
-9
-10
-11
-12
Henkes et al. (2014)
Passey & Henkes (2012)
This study

1. Download high-res image (340KB)
2. Download full-size image

Fig. 3. Clumped isotope results for heating experiments on optical calciteunder wet-HP conditions (P = 100 MPa). Symbols represent different experimental temperatures: green triangles are 385 °C, blue squares are 405 °C, black diamonds are 425 °C, and red circles are 450 °C. Error bars are one standard error. (a) The Δ_{47} values as a function of heating time, in absolute reference frame of Dennis et al. (2011). Each symbol represents an average of two analytical measurements adjusted for partial reprecipitation at the reaction temperature. The star indicates the Δ_{47} value of the starting material. (b) Reaction progress plotted as ln(1 − F) as a function of time. The dashed lines represent best-fit linear regressions following first-order behavior. Open symbols mark the early non-first-order reaction progress and were excluded from the regression analysis. The slopes of the lines are equivalent to the reaction rate constants *k*. The star indicates the starting material. (c) Arrhenius regression plot of optical calcite reacted under wet-HP conditions (this study), closed symbols outlined in black, and dry-LP conditions (Passey and Henkes, 2012), closed symbols, and brachiopods reacted under dry-LP conditions (Henkes et al., 2014), open symbols. Lines are best-fit linear regressions to the data: solid line is this study, long dashed line is Passey and Henkes (2012), and short-dotted line is Henkes et al. (2014). The slopes of the lines are proportional to the activation energy (E_a) and the intercepts are proportional to the pre-exponential factor (k_o). (For interpretation of the references to colour in this figure legend, the reader is referred to the web version of this article.)

This change in carbonate $\delta^{18}O$ is likely the result of exchange of oxygen between the carbonate and water, which initially are not in isotopic equilibrium at the experimental conditions (the initial isotopic difference between calcite and water is 27‰, whereas $1000\ln\alpha_{eq}$values are 3.5‰ and 2.4‰ at 385 and 450 °C, respectively, where α_{eq} is the equilibrium fractionation factor between calcite and water (O'Neil et al., 1969)). Oxygen exchange could occur, for example, through diffusion of oxygen into and out of the carbonate, or through dissolution and reprecipitation reactions at the calcite–water interface. We calculated expected changes in carbonate $\delta^{18}O$ values as a result of diffusion using oxygen self-diffusion coefficients reported by Farver (1994) and assuming a simple cube geometry for our 0.250–0.125 mm mesh size samples (see Appendix A for details of the calculation). Based on this, we predicted a change in carbonate $\delta^{18}O$ of less than 0.02‰ for the highest reaction temperature (450 °C). The larger (up to 0.6‰) decrease that we observed indicates a different process than diffusion alone is altering the oxygen isotopic composition of the calcite, such as dissolution–reprecipitation reactions. SEM images of unreacted and reacted samples

(Figs. S1–S6 in Supplementary Material) were consistent with this suggestion, with reacted samples showing minor morphological changes such as rounded edges and etch pits. These features were not prevalent in the starting material.

For the 450 °C reaction temperature, the attainment of isotopic equilibrium between the calcite and water contained inside each reaction capsule would result in a lowering of calcite $\delta^{18}O$ by approximately 18.5‰, from a starting composition of 21.2‰ VSMOW (=−9.49‰ VPDB) to an equilibrium composition of 2.7‰ VSMOW (=−27.4‰ VPDB). These numbers were calculated using the equilibrium calcite-water temperature-dependent fractionation relation of O'Neil et al. (1969), and take into account the molar quantity of oxygen in the water versus mineral in our experiments. The maximum observed change in calcite $\delta^{18}O$ of 0.6‰ corresponds to less than 3.5% reaction progress for exchange of oxygen between calcite and capsule water.

Although minor, the reactions suggested by this shift in $\delta^{18}O$, be they dissolution-precipitation reactions, precipitation of new mineral, or solid-state reactions, could be problematic for the interpretation of our clumped isotope results because the newly-formed calcite would likely have an equilibrium Δ_{47} value similar to the reaction temperature. In other words, our measured Δ_{47} values would reflect a combination of the solid-state reordering process (as intended) and dissolution–reprecipitation reactions (unintended). For the case that reprecipitation did occur, we can estimate the effect that this would have on measured Δ_{47} values using a mass balance approach:

$$\Delta47meas = fprecip\,\Delta47precip + (1-fprecip)\,\Delta47corrected \quad (3)$$

where f_{precip} is the fraction of the mineral volume that is newly precipitated, $\Delta47precip$ is the precipitated Δ_{47} value in equilibrium with the reaction temperature, $\Delta47meas$ is the measured Δ_{47} value, and $\Delta47corrected$ is the Δ_{47} value that is corrected for the influence of dissolution–reprecipitation on the surface of the mineral. $\Delta47meas$ is a measured parameter and $\Delta47precip$ can be estimated for the specific reaction temperature using a clumped-isotope temperature calibration (here, Eq. (5) of Passey and Henkes, 2012). The parameter f_{precip} can be calculated for each sample based on the reaction progress observed for $\delta^{18}O$ as discussed above. This leaves $\Delta47corrected$ as the only unknown. The average difference between $\Delta47corrected$ and $\Delta47meas$ was 0.002‰, with the difference ranging from 0.007‰ to 0.0001‰ (Table 1).

We also calculated the influence of two-component mixing on Δ_{47}values using the nonlinear mixing model of Defliese and Lohmann (2015). The difference between the nonlinear mixing model and the linear mixing model (Eq. (3)) was less than 0.0015‰ for the extreme case that the calcite consisted of a mixture of 4% mineral in clumped isotope equilibrium and oxygen-isotope equilibrium with water at 450 °C ($\delta^{13}C$ = −4.7‰

(VPDB), $\delta^{18}O$ = −33.5‰ (VPDB), Δ_{47} = 0.32‰ (ARF)), and 96% mineral of the initial isotopic composition ($\delta^{13}C$ = −4.7‰, $\delta^{18}O$ = −9.5‰, Δ_{47} = 0.63‰).
Such corrections are smaller than the analytical precision of the isotopic analysis (~0.015‰, 1σ), and thus these corrections are unimportant for any of our interpretations. Nevertheless, we view the Δ47corrected values calculated from the linear mixing model as a more accurate representation of the true Δ_{47} due to reorder processes versus the Δ47meas values, and hence we use the Δ47corrected values for calculations and figures in the remainder of this paper. We note that it is also possible that the change in $\delta^{18}O$ of calcite underestimates the actual amount of mineral-fluid interaction, and hence clumped-isotope reordering. This could arise if the same discrete atoms of oxygen were exchanged multiple times between mineral and surface species but at different site locations on the mineral surface each exchange (for example, in the case of a tightly-bound hydration layer). In this scenario, the reaction progress for clumped-isotope reordering would be greater than the apparent reaction progress for oxygen isotope exchange (as gauged by the change in $\delta^{18}O$). We cannot quantify the extent to which this type of process may have influenced our samples, so we leave this as a hypothesis that could possibly be revisited by future work.
The initial clumped-isotope composition of MGB-CC-1 is Δ_{47} = 0.634 ± 0.01‰, (1σ) and heated samples ranged from Δ_{47} = 0.309–0.594‰. The Δ_{47} values of heated samples decreased with increasing reaction duration in all experiments (Fig. 3a). Additionally, the rate of change increased with increasing temperature. Samples held at 450 °C for reaction times of at least 48 h were within error of the expected equilibrium Δ_{47} value at the experimental temperature. Samples held at lower reaction temperature did not reach equilibrium Δ_{47} values, consistent with results from previous studies of Passey and Henkes (2012) and Henkes et al. (2014) (*i.e.*, the kinetics are too slow for these experiments to reach equilibrium on laboratory timescales of several weeks or less).

4. Discussion, wet versus dry reordering rates

We modeled the experimental Δ_{47} data to extract the kinetic parameters using two different kinetic models, the first-order approximation model of Passey and Henkes (2012), and the 'paired reaction-diffusion model' of Stolper and Eiler (2015). A detailed description of these models and the differences between them is given in Stolper and Eiler (2015; p. 385–388), but we provide a brief summary here. The first-order approximation model posits that clumped-isotope reordering is enabled by transient defects (defects which are progressively inactivated during heating, for example, by annealing) and 'equilibrium defects', the concentration of which is constant through the

course of the reaction. The initial fast reordering is due to the combined activity of the transient and equilibrium defect pools, and the pseudo first-order kinetics arising from the equilibrium defect pool as it becomes the dominant mechanism of reordering once the transient defects have been annealed. In the first-order approximation model, the transient phase of the reaction is ignored, and rate constants are determined only for the equilibrium component of the reaction. The transient-defect/equilibrium-defect model of Henkes et al. (2014) is essentially the same in concept as the "first-order approximation" model, and differs from the latter only in that it explicitly models the transient phase of the reaction.

The paired reaction-diffusion model (Stolper and Eiler, 2015) posits that there are two factors that control the rate of solid-state reordering, isotope exchange between adjacent carbonate ions, and a short-range volume diffusion mechanism. During the initial heating of the sample, ^{13}C–^{18}O bonds are quickly destroyed by isotope-exchange reactions between local carbonate groups. This is manifested in the experiments as the initial fast change in Δ_{47} values. However, this leads to buildup of pairs (a pair comprises adjacent, singly isotopically substituted carbonate ions, one with ^{13}C, and the other with ^{18}O), which can back-react to reform clumped carbonate groups. This has the effect of retarding the net rate of clump dissociation, leading to a slower reordering rate following the initial period of fast reordering. A pseudo first-order reaction progress later emerges after the pair concentration relaxes towards equilibrium and the short-range volume diffusion mechanism becomes predominant.

We have insufficient data for the early reaction (<120 min) to use the transient-defect/equilibrium defect model of Henkes et al. (2014). With respect to the two models we do use ("first-order approximation" and "paired reaction-diffusion"), our intent is not to evaluate the models themselves, but rather to compare wet and dry reordering kinetics in the context of available model frameworks.

4.1. Comparison of reordering kinetics for wet vs. dry conditions using the first-order approximation model

The bond reordering reaction progress for the pseudo first-order model of Passey and Henkes (2012) is described by the following equation:

$$(4)\ln\Delta47t-\Delta47eq\Delta47init-\Delta47eq=\ln1-\Delta47init-\Delta47t\Delta47init-\Delta47eq=\ln[1-F]=-kt$$

where

$$(5)F=\Delta47init-\Delta47t\Delta47init-\Delta47eq$$

and $\Delta47init$ is the initial value of the sample, $\Delta47t$ is the value of the sample at a given temperature T for a period of time t, $\Delta47eq$ is the theoretical value for a sample in

equilibrium at a given temperature T, and k is the reaction rate. Equilibrium Δ_{47} values as a function of temperature were calculated according to Eq. (5) of Passey and Henkes (2012). Linear fits to the first-order reaction progress for each temperature yield slopes that correspond to k at that temperature (Fig. 3b). The slope of a linear regression of ln(k) versus 1/T from the various experiments yields the activation energy, E_a, and the y-intercept is ln(k_o). The Arrhenius equation is:

(6)k=koexp-EaRT

where k is the reaction progress rate constant, R is the gas constant, and T is the temperature in kelvins (Fig. 3c). This is equivalent to

(7)k=krefexpEaR1Tref-1T

when $T_{ref} = \infty$. Solving for k_o in Eq. (6) involves an extrapolation well outside of the experimental temperature range, and hence the $k_o$value has a large associated error. In contrast, if T_{ref} of Eq. (7) is within the range of experimental temperatures, the calculation of $k_{ref}$is based on interpolation within the experimental dataset, and the associated error is considerably smaller. Therefore, we use T_{ref} = 415 °C, which is centered within our range of experimental temperatures, and we calculate the corresponding k_{ref} following methods outlined in Passey and Henkes (2012). Regressions were carried out using error weighted least squares regression using the statistical software JMP.

Consistent with previous studies (Passey and Henkes, 2012, Henkes et al., 2014, Stolper and Eiler, 2015), we observed non-zero intercepts and a 'kink' in reaction progress in plots of first-order reaction progress (Fig. 3b), in the interpretative frame work of this model, this would represent the proposed initial fast reordering to the putative transient defect pool. The kink is subtle in our dataset because we have only one time-point (120 min) within the period of initial fast reordering, whereas the studies of Passey and Henkes (2012) and Henkes et al. (2014) were able to better define the kink with observations at ~30, 60, and 120 min.

Samples reacted under wet-HP and dry-LP conditions had similar, but statistically different Δ_{47} values. The Δ_{47} values for wet-HP samples were consistently lower than Δ_{47} values for samples reacted under dry-LP conditions at any particular temperature and reaction time except for a single dry-LP data point. Reaction progress for wet-HP samples followed the same trends as dry-LP samples, but wet-HP reaction progress occurred faster than dry-LP (Fig. 4 and Table 2). Rates for wet-HP conditions are consistently two to three times higher than dry-LP conditions regardless of whether short reaction time data was included or excluded from the regression analysis(Table 2). The intercepts of the first-order reaction progress regressions (Fig. 4b) are broadly similar for wet and dry experimental data at any given reaction temperature, suggesting

that the initial fast reordering mechanism(s) was not strongly influenced by the presence of water.

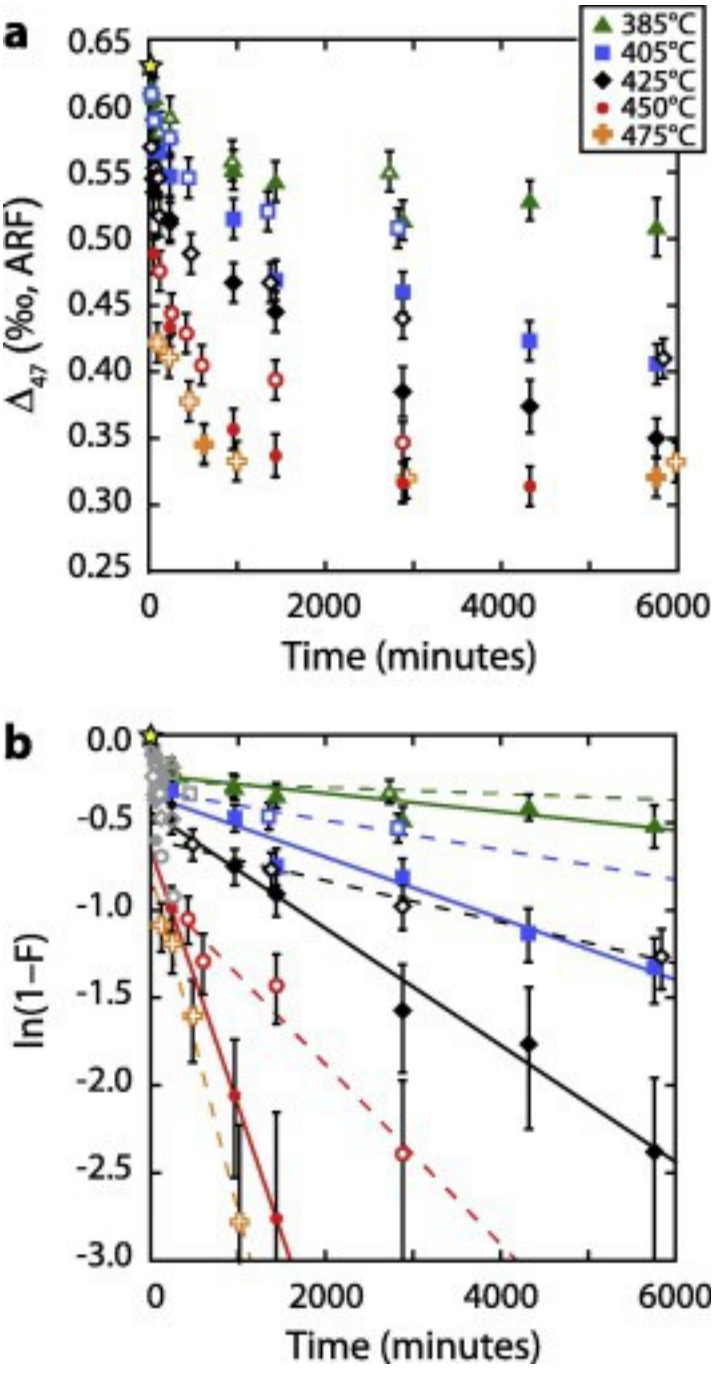

1. Download high-res image (291KB)
2. Download full-size image

Fig. 4. Comparison of heating experiments on optical calcite under wet-HP conditions (P = 100 MPa, filled symbols) and dry-LP conditions (P = 0.1 MPa, open symbols) of Passey and Henkes (2012). Symbols represent different experimental temperatures:

green triangles are 385 °C, blue squares are 405 °C, black diamonds are 425 °C, red circles are 450 °C, and orange crosses are 475 °C. Also shown are results for wet, low-pressure (P = 0.1 MPa) experiments at 475 °C (orange, closed crosses) (Passey and Henkes, 2012). Error bars are one standard error. a) The Δ_{47} values as a function of heating time, in absolute reference frame of Dennis et al. (2011). Each symbol represents an average of two analytical measurements. The wet-HP data are adjusted for partial reprecipitation at the reaction temperature. The star indicates the Δ_{47} value of the starting material. (b) Reaction progress ln(1 − F) plotted as a function of time. The lines represent best-fit linear regressions following first-order behavior: solid lines are this study and dashed lines are Passey and Henkes (2012). Grey symbols did not exhibit first-order behavior and were excluded from the regression analysis. (For interpretation of the references to colour in this figure legend, the reader is referred to the web version of this article.)

Table 2. First-order approximation model reaction progress rate constants and Arrhenius parameters for optical calcite reordering experiments for wet-HP reactions (this study) and dry-LP reactions (Passey and Henkes, 2012). Arrhenius parameters for Permian brachiopod calcite reacted under dry-LP conditions (Henkes et al., 2014) are included for comparison. All regressions exclude the initial rapid reordering component of reaction data.

***T* (°C)**	**Slope (=*k*) (s^{-1})**	**Intercept**	***R*²**	**Stats**
Optical calcite (aqueous, P = 100 MPa) – this study				
385	$-8.82\ (\pm2.5) \times 10^{-7}$	−0.24 (±0.04)	0.76	a, c, e
405	$-3.06\ (\pm0.36) \times 10^{-6}$	−0.33 (±0.06)	0.95	a, c, e
425	$-5.82\ (\pm0.35) \times 10^{-6}$	−0.41 (±0.04)	0.99	a, c, e
450	$-2.54\ (\pm0.01) \times 10^{-5}$	−0.63 (±0.002)	1.00	a, c, e
Arrhenius regression: E_a = 209 ± 16 kJ/mol			0.99	a, c, e
$k_o = 3.08 \times 10^{10}\ s^{-1}\ [(+38.8/-2.85) \times 10^{10}]$				
$k_{ref} = 4.42\ (\pm0.51) \times 10^{-6}\ s^{-1}$				
Optical calcite (dry, P = 0.1 MPa) –Passey and Henkes (2012)				
385	$-3.27\ (\pm0.42) \times 10^{-7}$	−0.27 (±0.03)	–	–
405	$-1.40\ (\pm0.15) \times 10^{-6}$	−0.32 (±0.04)	0.99	b, d, f
425	$-2.02\ (\pm0.17) \times 10^{-6}$	−0.59 (±0.02)	0.99	a, c, e
450	$-8.00\ (\pm1.72) \times 10^{-6}$	−0.88 (±0.12)	0.91	a, c, e
475	$-3.00\ (\pm0.39) \times 10^{-5}$	−0.79 (±0.09)	0.97	a, c, e
Arrhenius regression: E_a = 196 ± 18 kJ/mol			0.97	a, c, e
$k_o = 1.27 \times 10^{9}\ s^{-1}\ [(+29.2/-1.22) \times 10^{9}]$				
$k_{ref} = 1.69\ (\pm0.23) \times 10^{-6}\ s^{-1}$				

T (°C)	Slope (=k) (s^{-1})	Intercept	R^2	Stats
Permian brachiopod calcite (dry, P = 0.1 MPa) –Henkes et al. (2014)				
385	-5.75×10^{-7}	−0.34	–	–
405	-2.02×10^{-6} (± 0.32) $\times 10^{-6}$	−0.37 (±0.04)	0.98	b, d, f
425	-3.72×10^{-6} (± 0.11) $\times 10^{-6}$	−0.58 (±0.02)	1.00	a, c, e
450	-1.10×10^{-5}	−0.69	–	–
475	-3.10×10^{-5} (± 0.35) $\times 10^{-6}$	−0.81 (±0.06)	0.99	b, c, f
Arrhenius regression: E_a = 177 ± 8 kJ/mol			0.99	a, c, e
$k_o = 7.34 \times 10^7$ s^{-1} [(+20.4/−5.40) $\times 10^7$]				
$k_{ref} = 2.53$ (± 0.25) $\times 10^{-6}$ s^{-1}				

Note: Regression analysis followed error weighted least squares regression using statistical software JMP. Error (±) is reported as one standard error. All k_{ref} values were evaluated at T_{ref} = 415 °C. The error for k_{ref} is reported as the mean relative error of the temperature specific rate constants.

a: Regression ANOVA *F*-ratio statistic significant at the 0.05 level.

b: Regression ANOVA *F*-ratio statistic significant at the 0.1 level.

c: Slope significantly different from zero based on the Student *t*-distribution at 0.05 level.

d: Slope significantly different from zero based on the Student *t*-distribution at 0.1 level.

e: Intercept significantly different from zero based on the Student *t*-distribution at 0.05 level.

f: Intercept significantly different from zero based on the Student *t*-distribution at 0.1 level.

We compared the Δ_{47} values of marble (NBS-19, HAF Carrara) and low temperature carbonate (102-GC-AZ01) standards analyzed during each analytical session in order to rule out instrumental drift as a possible explanation for the difference in Δ_{47} for the two different reaction conditions. Standards analyzed during wet-HP sample analytical sessions (January, 2015 through April, 2015) averaged Δ_{47}= 0.391 ± 0.013 and Δ_{47} = 0.695 ± 0.014 (1σ) for marble and low temperature standards, respectively (Table 1). Standards analyzed during dry-LP sample analytical sessions (February, 2011 through August, 2011) averaged Δ_{47} = 0.392 ± 0.019 and Δ_{47} = 0.705 ± 0.012 (1σ) for marble and low temperature standards, respectively. The difference in Δ_{47} values between samples reacted under wet-HP and dry-LP conditions increased with reaction duration from 0.010‰ to 0.069‰, with an average offset of 0.029‰, with the wet-HP values being lower in Δ_{47} at a given time point than the dry-LP for an equivalent experimental temperature. This average difference (0.029‰) is ~3x larger than the difference we observe for standards analyzed during the two different studies. Therefore, we do not attribute the difference in Δ_{47} values between wet-HP and dry-LP reaction conditions to offsets in Δ_{47} measurements between analytical sessions.

Fig. 4 includes data for two 475 °C wet, low-pressure reactions, heated for 631 and 5757 min, from Passey and Henkes (2012). These are the same MGB-CC-1 optical calcite as used in our study, but they were reacted under wet, *low-pressure* (0.1 MPa) conditions. There was no significant difference between wet and dry conditions for the sample heated at 475 °C for 5757 min (*i.e.*, >3.5 days). This is not surprising because samples reacted at 475 °C had already reached equilibrium by this time. The sample heated at 475 °C under wet, low-pressure conditions for 631 min did not noticeably differ from the reaction progress suggested by samples reacted under dry, low-pressure conditions. Additionally, wet-HP experiments on the NE-CC-1 spar calcite of Passey and Henkes (2012) did not show clear differences in reordering rates from dry-LP experiments. The spar calcite had variable concentrations of Mg and Mn, and had reordering kinetics suggestive of a two-component system, and thus it is not directly comparable to our experiments on low Mg, low Mn optical calcite. Although the datasets are small for both of these preliminary experiments, they do suggest the possibility that pressure or mineral composition has an influence on the response of reordering rates to wet versus dry conditions.

Wet-HP reaction rates for each temperature were faster than rates for dry-LP conditions. The k_{ref} values, calculated at 415 °C, were 4.42 (±0.51) × 10^{-6} s^{-1} and 1.69 (±0.23) × 10^{-6} s^{-1} for wet-HP and dry-LP conditions, respectively, where the error for k_{ref} is reported as the mean relative error of the temperature specific rate constants.

Thus k_{ref} values for wet and dry conditions are significantly different, with k_{ref} values for wet-HP conditions 2.6 ± 0.5 times greater than k_{ref}values for dry-LP conditions (Table 2, Table 4). Statistics for the linear regressions are included in Table 2. The difference between wet-HP and dry-LP reaction conditions was not resolvable with k_o values because the associated error, after extrapolation to $T_{ref} = \infty$, was too large. The activation energies for wet-HP and dry-LP reaction conditions were identical, within error. The activation energies and pre-exponential factors, respectively, were E_a = 209 ± 16 kJ/mol and k_o = 3.08 × 10^{10} s^{-1} [(+38.8/−2.85) × 10^{10}] for wet-HP conditions and E_a = 196 ± 18 kJ/mol and k_o = 1.27 × 10^{9} s^{-1} [(+29.2/−1.22) × 10^{9}] for dry-LP where k_o is the rate constant at infinite temperature (Table 2).

4.2. Paired reaction-diffusion model comparison of wet-HP and dry-LP conditions on clumped isotope bond reordering

Here we use the paired reaction-diffusion model of Stolper and Eiler (2015) to derive rate constants for our data, and we compare the results to those for dry-LP conditions of the same optical calcite as previously modeled by Stolper and Eiler (2015). Rate

constants are listed in Table 3. The model is based on an expansion of Eq. (1) into two reactions:

(8)12C16O32-+12C16O218O2-↔pair

and

(9)pair↔13C16O3,single2-+12C16O218Osingle2-

where pair refers to adjacent 12C16O32- and 12C16O218O2- groups and single refers to a species with single isotopic substitution that does not have another singly isotopically substituted species in an adjacent location in the crystal lattice. Reaction progress in the paired reaction-diffusion model is described by the following equations (Stolper and Eiler, 2015):

(10)dξdt=kf12C16O32-o13C16O218O2-o-ξ-kb[pair]t

and

(11)dpairdt=kf12C16O32-o13C16O218O2-o-ξ-kb[pair]t+kdif-single12C16O218O2-single,o13C16O32-single,o-kdif-pair[pair]t

where ξ is the reaction progress that tracks the change in $^{13}C^{16}O_2^{18}O^{2-}$ with time *t*, and k_f and k_b represent the rate constants for the forward and backward isotope exchange reactions, respectively, at time *t*. The rate constants for the diffusion component are represented by $k_{dif\text{-}single}$ and $k_{dif\text{-}pair}$ for singles and pairs, respectively, where single refers to a singly substituted carbonate group that is not adjacent to another singly substituted carbonate group.

Table 3. Rate constants derived from modeling reaction progress following the pair reaction-diffusion model of Stolper and Eiler (2015) for optical calcitereordering under wet, high pressure conditions (this study). For comparison, data for dry, low pressure conditions are shown for optical calcite (Passey and Henkes, 2012) and Permian brachiopod calcite (Henkes et al., 2014), and dry, mid-pressure conditions for optical calcite (Stolper and Eiler, 2015).

***T* (°C)**	**k_f (sec^{-1})**	**$k_{dif\text{-}single}$ (sec^{-1})**	***R*²**	**Stats**
Optical calcite (aqueous, P = 100 MPa) – this study				
405	9.09 (±1.10) × 10^{-4}	1.84 (±0.091) × 10^{-5}	0.94	
425	3.34 (±0.385) × 10^{-4}	4.28 (±0.134) × 10^{-5}	0.98	
450	6.66 (±0.025) × 10^{-4}	2.41 (±0.012) × 10^{-4}	0.99	
Arrhenius regression (k_f): E_a = 165 ± 28 kJ/mol			0.97	b, e, h
k_o = 5.84 × 10^8 s^{-1} [(+63.5/−0.578) × 10^9]				
k_{ref} = 1.68 (±0.40) × 10^{-4} s^{-1}				
Arrhenius regression ($k_{dif\text{-}single}$): E_a = 249 ± 29 kJ/mol			0.99	b, e, h
k_o = 2.41 × 10^{14} s^{-1} [(+32.7/−0.239) × 10^{15}]				

T (°C)	k_f (sec^{-1})	$k_{dif\text{-}single}$ (sec^{-1})	R^2	Stats
k_{ref} = 2.95 (±0.25) × 10^{-5} s^{-1}				
Optical calcite (dry, P = 50–65 MPa) –Stolper and Eiler (2015)				
430	9.25 (±0.231) × 10^{-5}	6.83 (±0.046) × 10^{-6}		
536	3.64 (±0.054) × 10^{-3}	2.74 (±0.142) × 10^{-3}		
692	0.270 (±0.002)	0.128 (±0.001)		
Arrhenius regression (k_f): E_a = 172 ± 3 kJ/mol			1.00	a, d, g
k_o = 5.36 × 10^{8} s^{-1} [(+2.67/−1.78) × 10^{8}]				
k_{ref} = 4.72 (±0.22) × 10^{-5} s^{-1}				
Arrhenius regression ($k_{dif\text{-}single}$): E_a = 211 ± 18 kJ/mol			0.99	a, d, h
k_o = 5.33 × 10^{10} s^{-1} [(+66.3/−4.94) × 10^{10}]				
k_{ref} = 5.10 (±0.36) × 10^{-6} s^{-1}				
optical calcite (dry, P = 0.1 MPa) –Passey and Henkes (2012)				
405	8.17 (±0.217) × 10^{-5}	5.86 (±0.328) × 10^{-6}		
425	2.97 (±0.040) × 10^{-4}	2.13 (±0.030) × 10^{-5}		
450	4.94 (±0.262) × 10^{-4}	2.02 (±0.101) × 10^{-4}		
475	5.83 (±0.046) × 10^{-4}	3.06 (±0.038) × 10^{-4}		
Arrhenius regression (k_f): E_a = 93 ± 27 kJ/mol			0.85	b, e, i
k_o = 1.78 × 10^{3} s^{-1} [(+16.2/−0.176) × 10^{4}]				
k_{ref} = 1.71 (±0.17) × 10^{-4} s^{-1}				
Arrhenius regression ($k_{dif\text{-}single}$): E_a = 231 ± 37 kJ/mol			0.95	a, d, g
k_o = 4.93 × 10^{12} s^{-1} [(+210/−0.492) × 10^{13}]				
k_{ref} = 1.36 (± 0.18) × 10^{-5} s^{-1}				
Permian brachiopod calcite (dry, P = 0.1 MPa) –Henkes et al. (2014)				
405	6.92 (±0.291) × 10^{-5}	8.41 (±0.715) × 10^{-6}		
425	2.84 (±0.084) × 10^{-4}	3.42 (±0.082) × 10^{-5}		
450	8.07 (±0.545) × 10^{-4}	1.19 (±0.046) × 10^{-4}		
475	1.23 (±0.034) × 10^{-3}	5.78 (±0.147) × 10^{-4}		
Arrhenius regression (k_f): E_a = 165 ± 28 kJ/mol			0.95	a, d, g
k_o = 5.13 × 10^{8} s^{-1} [(+58.3/−0.509) × 10^{9}]				
k_{ref} = 1.46 (±0.24) × 10^{-4} s^{-1}				
Arrhenius regression ($k_{dif\text{-}single}$): E_a = 248 ± 11 kJ/mol			1.00	a, d, g
k_o = 1.18 × 10^{14} s^{-1} [(+6.82/−1.01) × 10^{14}]				

T (°C)	k_f (sec^{-1})	$k_{dif\text{-}single}$ (sec^{-1})	R^2	Stats

k_{ref} = 1.75 (±0.30) × 10^{-5} s^{-1}

Note: Error (±) is reported as one standard error. Regression analysis followed error weighted least squares regression using statistical software JMP. The error for k_{ref} is reported as the mean relative error of the temperature specific rate constants. All k_{ref}values were evaluated at T_{ref} = 415 °C.

a: Regression ANOVA *F*-ratio statistic significant at the 0.05 level.

b: Regression ANOVA *F*-ratio statistic significant at the 0.1 level.

c: Regression ANOVA *F*-ratio statistic significant at the 0.2 level.

d: Slope significantly different from zero based on the Student *t*-distribution at 0.05 level.

e: Slope significantly different from zero based on the Student *t*-distribution at 0.1 level.

f: Slope significantly different from zero based on the Student *t*-distribution at 0.2 level.

g: Intercept significantly different from zero based on the Student *t*-distribution at 0.05 level.

h: Intercept significantly different from zero based on the Student *t*-distribution at 0.1 level.

i: Intercept significantly different from zero based on the Student *t*-distribution at 0.4 level.

We converted our Δ_{47} values from the absolute reference frame to the Ghosh reference frame following the approach of Stolper and Eiler (2015) because the model and rate constants in Stolper and Eiler (2015) were calculated within the Ghosh reference frame. Briefly, we used a transfer function based on an extensive set of clumped-isotope data of Henkes et al. (2014) given in both reference frames, where Δ_{47} values of carbonate standards NBS-19 and 102-GC-AZ01 (an internal standard) in the Ghosh reference frame were identical, within error, to values determined at Caltech. After application of the transfer function, we subtracted 0.011‰ from the Johns Hopkins data to account for the difference in acid fractionationfactors used in the Henkes et al. (2014) study and the Stolper and Eiler (2015) study. We then calculated the concentration of pairs for each experimental temperature using Eq. (17) of Stolper and Eiler (2015). Finally, we used Matlab's ordinary differential equation solver ODE45 to fit our data, following the methods of Stolper and Eiler (2015).

The computational results of the paired model fits to our experimental datasets and kinetic parameters are shown in Fig. 5 and Table 3. The temperature specific rate constants under wet-HP and dry-LP conditions were indistinguishable for the exchange component (k_f) at 405 °C and 425 °C and the diffusional ($k_{dif\text{-}single}$) component at 450 °C. However, at 405 and 425 °C the rates for the diffusional ($k_{dif\text{-}single}$) component were ∼2 times higher for wet-HP conditions than dry-LP conditions, similar to our findings for the first-order approximation model. Furthermore, rates for the exchange (k_f) component under wet-HP conditions at 450 °C were ∼1.3 times higher than dry-LP conditions.

Linear fits to ln(k) versus 1/T followed the same trend as observed in previous studies (Fig. 6). There was no significant difference in activation energies between wet-HP and dry-LP reaction conditions for the diffusional ($k_{dif\text{-}single}$) component, but activation energies for the exchange (k_f) component were ∼2 times higher for wet-HP conditions compared with dry-LP conditions. In agreement with the first-order approximation model, the k_{ref} value, calculated at T = 415 °C, for the diffusional component of the paired model was higher for wet-HP conditions than dry-LP conditions. The k_{ref} values were 2.95 (±0.25) × 10^{-5} s^{-1} and 1.36 (±0.18) × 10^{-5} s^{-1} for wet-HP and dry-LP conditions, respectively, for the diffusional ($k_{dif\text{-}single}$) components for wet-HP and dry-LP conditions, respectively (Table 3, Table 4). Thus, diffusional k_{ref} values for wet-HP conditions were 2.2 ± 0.34 times greater than k_{ref} values for dry-LP conditions (Table 3, Table 4). The k_{ref} values for the exchange component were not significantly different for wet-HP and dry-LP conditions, 1.68 (±0.40) × 10^{-4} s^{-1} and 1.71 (±0.17) × 10^{-4} s^{-1}, respectively. Error for k_{ref} is reported as the mean relative error of the temperature specific rate constants. Statistics for the linear regressions are included in Table 3.

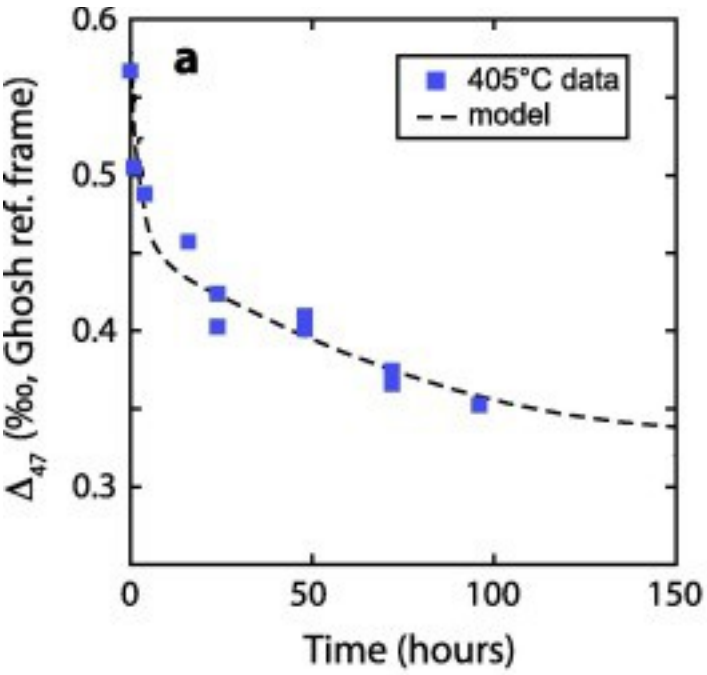
a
405°C data
model
0.6
0.5
0.4
0.3
Δ_{47} (‰, Ghosh ref. frame)
0
50
100
150
Time (hours)

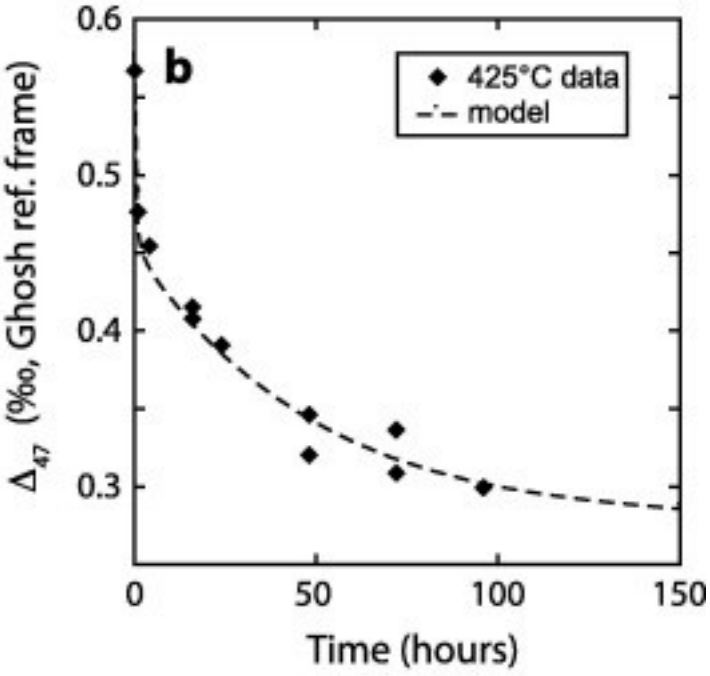
b
425°C data
model
0.6
0.5
0.4
0.3
Δ_{47} (‰, Ghosh ref. frame)
0
50
100
150
Time (hours)

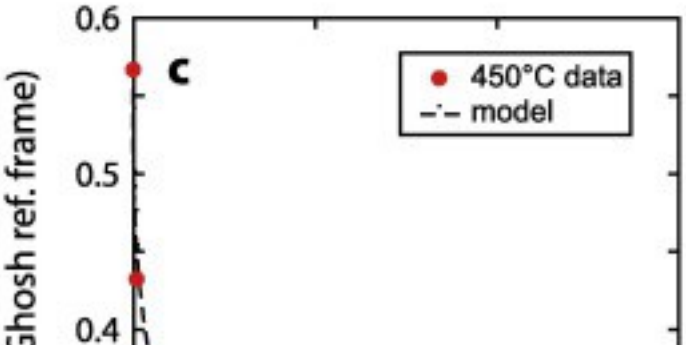
c
450°C data
model
0.6
0.5
0.4
ghosh ref. frame)

1. Download high-res image (255KB)
2. Download full-size image

Fig. 5. Paired model fits to wet-HP (P = 100 MPa) experimental data following methods of Stolper and Eiler (2015). Dashed lines are paired model fits and symbols are individual data points. These data were converted to the Ghosh reference frame from the absolute reference frame prior to model fitting. (a) model fit to 405 °C data (blue squares), (b) model fit to 425 °C data (black diamonds), (c) model fit to 450 °C data (red circles). (For interpretation of the references to colour in this figure legend, the reader is referred to the web version of this article.)

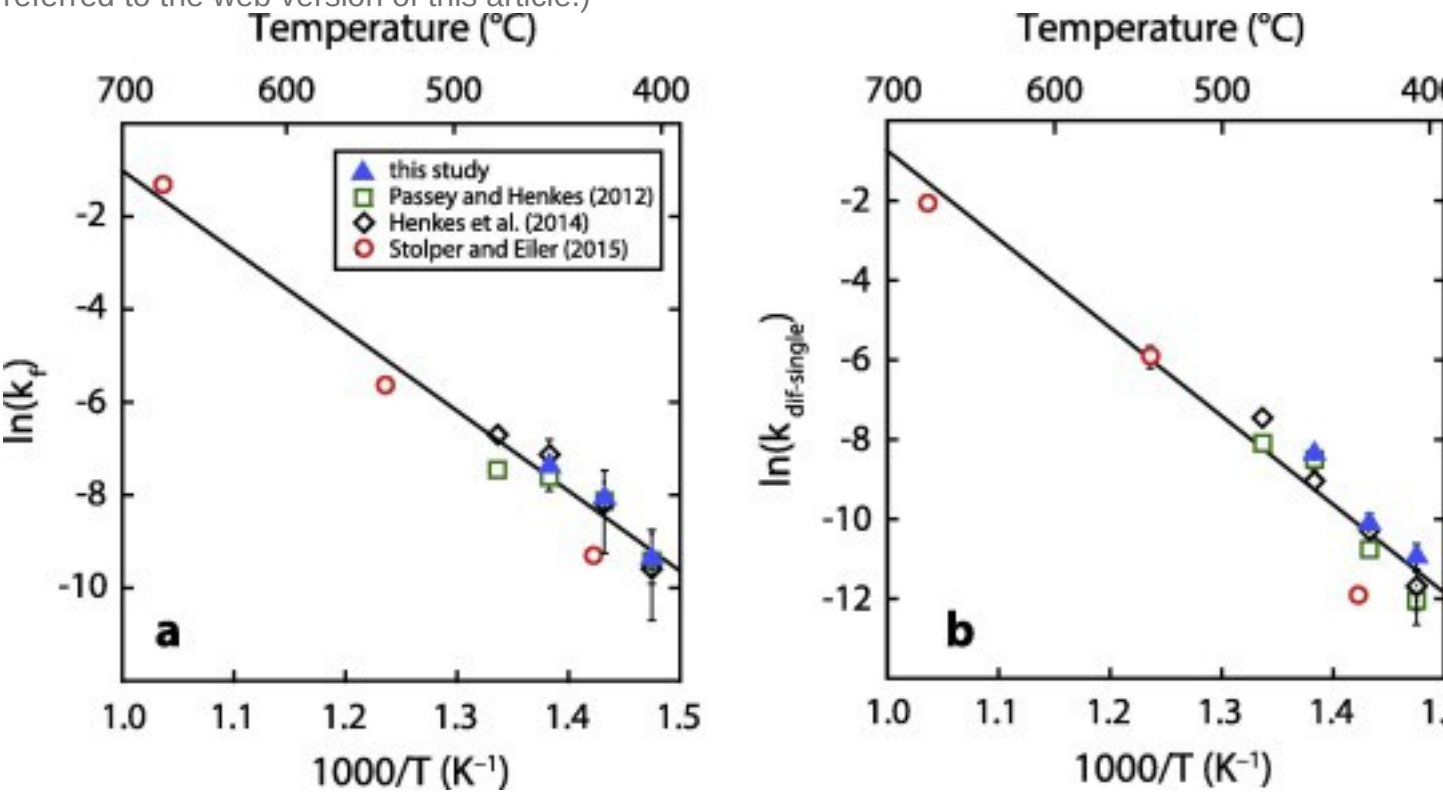

1. Download high-res image (218KB)
2. Download full-size image

Fig. 6. Arrhenius regression plot of bond reordering rate constants for calcitein the context of the paired reaction-diffusion model (Stolper and Eiler, 2015). Symbols refer to individual experimental data: closed blue triangles are wet-HP reaction conditions for this study; open green squares are Passey and Henkes (2012) data for optical calcite reacted under dry-LP conditions; open black diamonds are Henkes et al. (2014) data for brachiopods reacted under dry-LP conditions; and open red circles are Stolper and Eiler (2015) data for optical calcite reacted under dry, mid-pressure conditions (50–65 MPa). See Section for specific reaction conditions. Error bars represent 95% confidence intervals from Matlab's fitting routine. For symbols without error, the error is smaller than the size of the symbol. Lines are best-fit linear regressions to all of the data. (a) Results

for the exchange rate constant k_f. (b) Results for the diffusion-single rate constant $k_{dif\text{-}single}$. (For interpretation of the references to colour in this figure legend, the reader is referred to the web version of this article.)

Table 4. Summary of Arrhenius parameters for carbonates reacted in wet (DI water) or dry (CO_2) environments under high (P = 100 MPa), low (P = 0.1 MPa), or mid (P = 50–65 MPa) pressure conditions.

Conditions	Material	E_a(kJ/mol)	*Error*(±)	k_{ref}(s^{-1})	*Error*(±)	Reference
First-order approximation model				$\times10^{-6}$	$\times10^{-6}$	
wet-HP	Optical calcite	209	16	4.42	0.51	This study
dry-LP	Optical calcite	196	18	1.69	0.23	Passey and Henkes (2012)
dry-LP	Brachiopod calcite	177	8	2.53	0.25	Henkes et al. (2014)
Pair exchange-diffusion model						
Exchange component (k_f)				$\times10^{-4}$	$\times10^{-4}$	
wet-HP	Optical calcite	165	28	1.68	0.40	This study
dry-LP	Optical calcite	93	27	1.71	0.17	Passey and Henkes (2012)
dry-LP	Brachiopod calcite	165	28	1.46	0.24	Henkes et al. (2014)
dry-MP	Optical calcite	172	3	0.472	0.02	Stolper and Eiler (2015)
Diffusion component ($k_{diff\text{-}single}$)				$\times10^{-5}$	$\times10^{-5}$	
wet-HP	Optical calcite	249	29	2.95	0.25	This study
dry-LP	Optical calcite	231	37	1.36	0.18	Passey and Henkes (2012)
dry-LP	Brachiopod calcite	248	11	1.75	0.30	Henkes et al. (2014)
dry-MP	Optical calcite	211	18	0.510	0.04	Stolper and Eiler (2015)

Note: Regression analysis followed error weighted least squares regression using statistical software JMP. Error (±) is reported as one standard error. The first-order approximation model excluded initial non-first order reaction data. All k_{ref} values were evaluated at T_{ref} = 415 °C. The error for k_{ref} is reported as the mean relative error of the temperature specific rate constants.

The paired model produced a reasonable fit to the higher temperature datasets, but model fitting did not converge on either rate constant value (exchange k_f or diffusional $k_{dif\text{-}single}$) for the 385 °C dataset. We ran the model with various error parameters, for example both 1σ and 2σ analytical uncertainty for Δ_{47} values, and tested

model response when certain data points were excluded, for example measured data that fell greater than 2σ from original model outputs, and were unable to produce satisfactory results. Thus, model fitting of the lower temperature dataset is considered to be unsuccessful and is not included in Fig. 5 or Table 3, Table 4. The same issue was found in Stolper and Eiler (2015) when trying to fit the 385 °C experimental data of Passey and Henkes (2012) and Henkes et al. (2014).

5. Discussion, implications

5.1. Temperature–time reordering predictions

Here we illustrate the effect of wet-HP reaction conditions on carbonate clumped-isotope bond reordering rates relative to dry-LP conditions using the first-order approximation model and the pair exchange-diffusion model. Fig. 7 shows the temperature–time curves for 1% and 99% reaction progress for dry-LP and wet-HP kinetics of both models. Error for the reordering curves of both models is at a minimum near the temperature range of our experimental data.

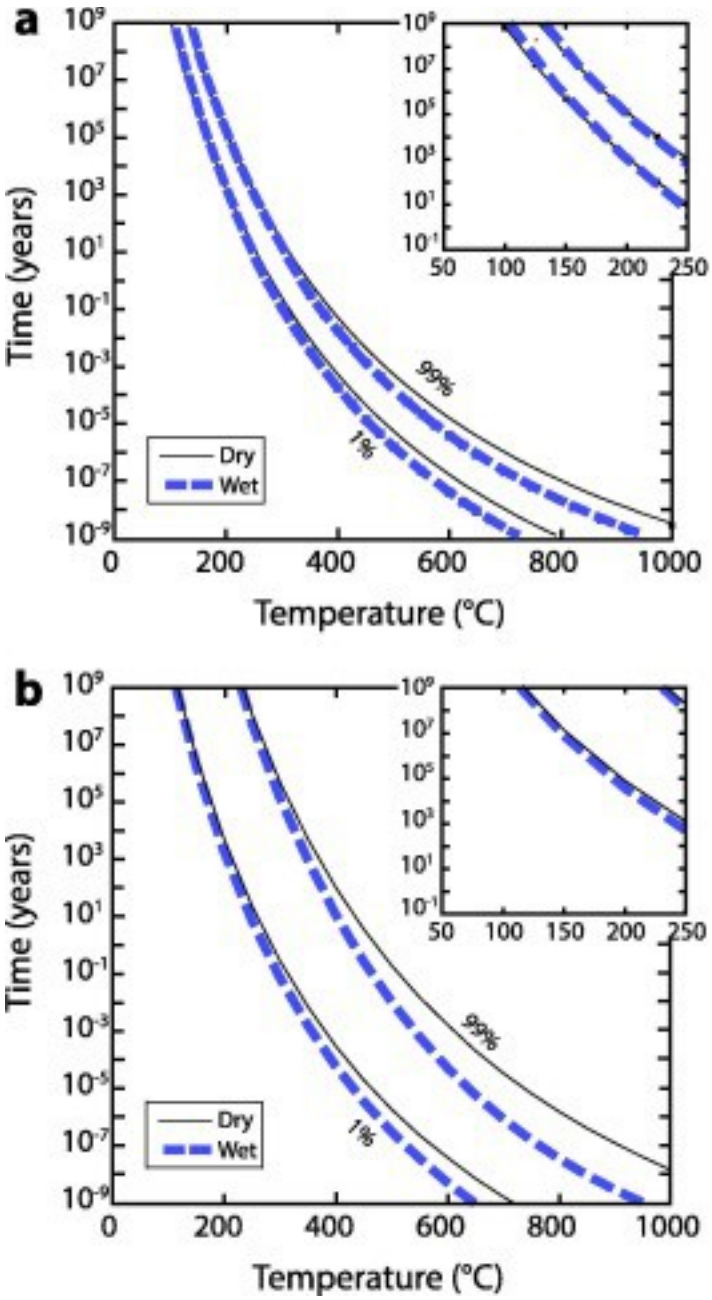

1. Download high-res image (294KB)
2. Download full-size image

Fig. 7. Temperature–time predictions for clumped-isotope bond reordering based on kinetic parameters for optical calcite MGB-CC-1. Curves represent 1% and 99% reordering. Think solid black lines are reordering curves based on the dry-LP kinetics of Passey and Henkes (2012) and thick dashed blue lines are based on the wet-HP kinetics of the current study. The insert illustrates conditions representative of typical sedimentary shallow crustal burial scenarios and highlights the similarity between reordering rates in wet-HP and dry-LP environments. The grey shaded region

represents error (1σ) for wet-HP calculations. (a) Reordering curves based on the first-order approximation model of Passey and Henkes (2012). (b) Reordering curves based on the pair exchange-diffusion model of Stolper and Eiler (2015). (For interpretation of the references to colour in this figure legend, the reader is referred to the web version of this article.)

For the first-order approximation model, we combined the bond reordering reaction progress (Eq. (4)) and the Arrhenius relation (Eq. (7)) following Henkes et al. (2014) to model the fractional extent of reordering as a function of both time and temperature independent of specific sample composition. The difference between the first-order approximation model wet-HP and dry-LP curves decreases with decreasing temperature and increasing time, and the associated error for each curve increases, resulting in nearly identical, within error, reordering predictions (Fig. 7a and Table 5). This includes geologically relevant temperature and time combinations of 10^{-1}–10^{9} years and 50–250 °C (Fig. 7a, insert). At short timescales and high temperature, the reordering curves for the first-order approximation model wet-HP and dry-LP conditions diverge. For timescales shorter than 10^{-3} years (*i.e.*, hours), the onset of bond reordering occurs at lower temperature in wet-HP conditions than dry-LP conditions (Fig. 7a and Table 5).

Table 5. Temperatures and time combinations for clumped-isotope reordering progress (1%, 50%, and 99%) in optical calcite based on the first-order approximation model of Passey and Henkes (2012) and the pair exchange-diffusion model of Stolper and Eiler (2015) for wet, high-pressure (100 MPa) kinetics of this study and dry, low-pressure (0.1 MPa) kinetics of Passey and Henkes (2012).

Time	**First-order approximation model**						**Pair exchange-diffusion model**					
	wet-HP (°C)			**dry-LP (°C)**			**wet-HP (°C)**			**dry-LP (°C)**		
	1%	**50%**	**99%**	**1%**	**50%**	**99%**	**1%**	**50%**	**99%**	**1%**	**50%**	**99%**
1 Ga	103	127	131	98	122	127	143	148	249	145	166	249
100 Ma	117	142	147	112	138	143	149	194	255	150	197	275
10 Ma	131	158	163	127	155	161	150	200	296	163	200	298
1 Ma	147	176	182	143	174	180	194	239	302	197	245	333
100 ka	163	195	201	161	195	201	200	250	346	200	267	350
10 ka	182	216	223	180	217	224	237	293	378	244	298	396
1 ka	201	239	247	201	242	249	249	323	399	260	343	440
100 years	223	265	273	224	269	277	291	350	445	298	386	487
10 years	247	292	301	249	299	309	315	398	490	340	436	539
1 year	273	323	333	277	333	344	349	448	538	381	492	596
1 month	304	361	372	311	374	387	398	514	595	433	560	679

Time	First-order approximation model						Pair exchange-diffusion model					
	wet-HP (°C)			dry-LP (°C)			wet-HP (°C)			dry-LP (°C)		
	1%	50%	99%	1%	50%	99%	1%	50%	99%	1%	50%	99%
1 day	353	421	434	365	441	456	483	618	695	503	689	813
1 h	407	487	503	426	517	536	573	741	827	627	842	987
1 min	492	595	616	522	643	668	731	952	1030	814	1134	1322
1 s	600	738	766	649	816	851	963	1299	1539	1116	1630	1963

For the pair exchange-diffusion model we simulated reordering from an initial starting temperature of −25 °C instantaneously heating over a range of final temperatures and tracked the fractional extent of reordering as a function of time. The 1% and 99% reordering curves of the pair exchange-diffusion model followed a similar trend as the first-order approximation model, but reordering occurred over a broader range of temperature–time combinations (Fig. 7b and Table 5). As with the first-order approximation model, the reordering curves for wet-HP and dry-LP conditions using the pair exchange-diffusion model diverged at high temperature and short timescales, but the difference between wet-HP and dry-LP curves was larger using the pair exchange-diffusion model compared with the first-order approximation model. For timescales shorter than 10^{-3} years, bond reordering approached equilibrium at lower temperature in wet-HP conditions than dry-LP conditions (Fig. 7b and Table 5). At low temperature and long timescales reordering curves for wet-HP and dry-HP conditions were nearly identical, within error. The pair exchange-diffusion modeled reordering curves indicated that a calcitecrystal held at 150 °C will be reordered to one percent of the equilibrium value at approximately ten million years for wet-HP and dry-LP kinetics, respectively, using the pair exchange-diffusion model compared with approximately one million years for both wet-HP and dry-LP kinetics using the first-order approximation model.

5.2. Cooling rate dependent blocking temperatures

Here we describe differences in cooling rate-dependent blocking temperatures (also known as “apparent equilibrium temperatures” and similar in concept to closure temperatures; see Passey and Henkes, 2012) for wet-HP and dry-LP reordering kinetics in terms of the first-order approximation model and the pair exchange-diffusion model. We modeled the change in Δ_{47} during cooling using a numerical approach to the first-order approximation model (Passey and Henkes, 2012):

(12)Δ47i=(Δ47i-1-Δ47eq,i)exp-ΔtkrefexpEaR1Tref-1T+Δ47eq,i

where Δ47i is the value of the calcite at time step *i*, Δ47eq,i is the equilibrium value at time step *i*, Δ_t is the time interval for each step, and *i* − 1 is the previous time step. The model was run until Δ47istabilized, with this value corresponding to the apparent equilibrium blocking temperature.

We ran the model using both wet-HP and dry-LP k_{ref} and E_a values over a wide range of cooling rates (Fig. 8a and b and Table 6). As the cooling rate increased, the blocking temperatures diverged with wet-HP kinetics yielding lower temperatures than dry-LP kinetics. The fastest modeled cooling rate, 1 °C/s, showed a difference of 47 °C in final blocking temperatures between wet-HP and dry-LP kinetics. The minimal difference in blocking temperatures between wet and dry regimes for slower cooling rates suggests that water has a negligible effect on clumped-isotope bond reordering over geologic timescales. Furthermore, typical analytical error of 0.015‰ for Δ_{47} values would not allow resolution of the difference between wet-HP and dry-LP blocking temperatures for slower cooling rates. For rapidly cooling processes (*e.g.*, lightning strikes, shear-heating, and contact metamorphism), the presence of water could yield a discernible offset in final observed Δ_{47} values compared with dry environments.

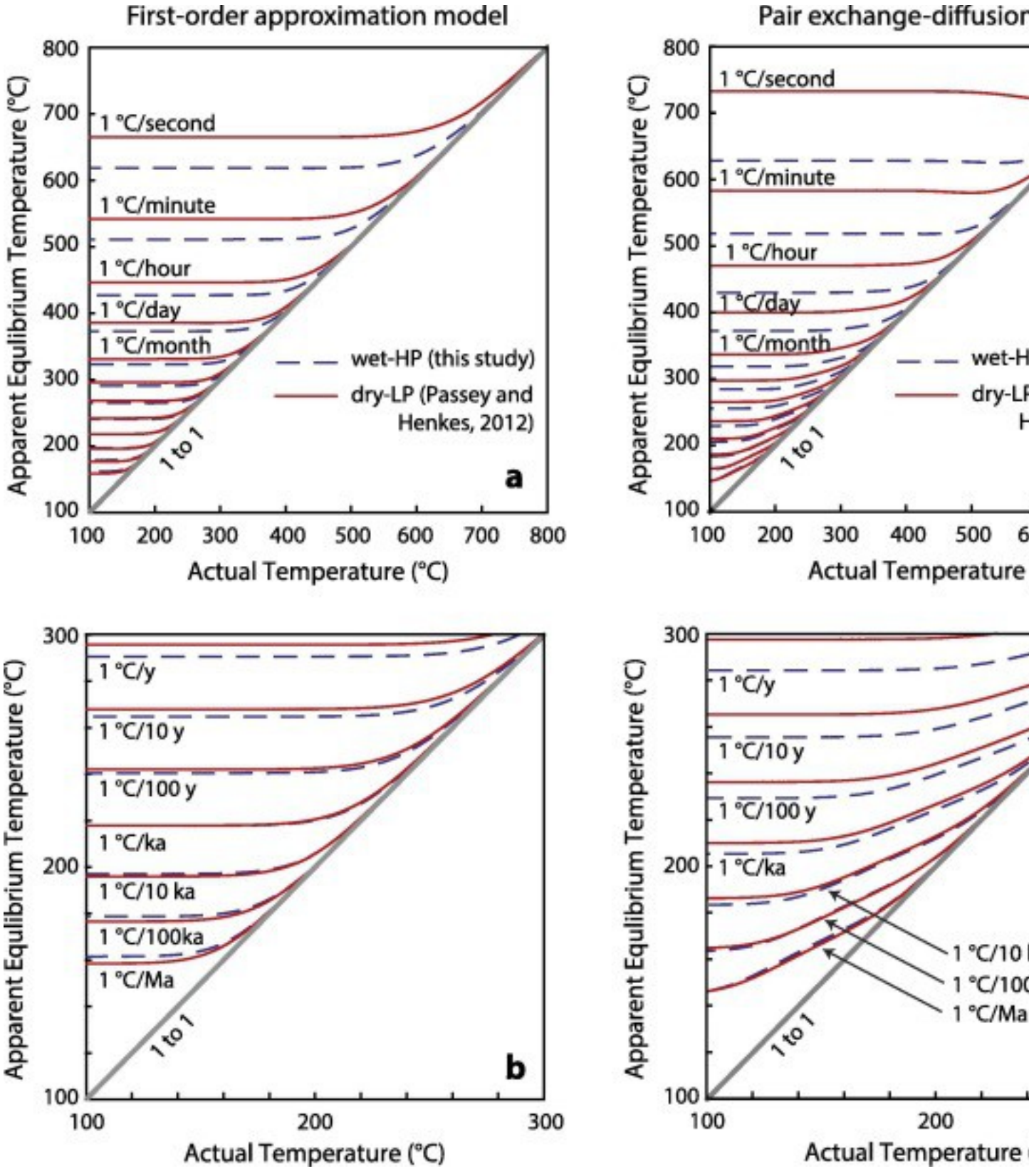

1. Download high-res image (833KB)

2. Download full-size image

Fig. 8. Cooling rate dependent blocking temperatures for calcite. Thin solid red lines are cooling curves based on dry-LP reordering kinetics of Passey and Henkes (2012), and blue dashed lines are cooling curves based on wet-HP reordering kinetics of this study. The thick solid grey line is the 1 to 1 line. (a) Curves for cooling rates of 1 °C/s, 1 °C/minute, 1 °C/hour, 1 °C/day, and 1 °C/month based on the first-order approximation model of Passey and Henkes (2012), (b) same as (a) but showing detail for slower cooling rates of 1 °C/year, 1 °C/10 years, 1 °C/100 years, 1 °C/ka, 1 °C/10 ka, 1 °C/100 ka, and 1 °C/1 Ma (c) curves for the same cooling rates as (a) but based on the pair exchange-diffusion model of Stolper and Eiler (2015), (d) same as (c) but showing detail for slower cooling rates of 1 °C/month, 1 °C/year, 1 °C/10 years, 1 °C/100 years, 1 °C/ka, 1 °C/10 ka, 1 °C/100 ka, and 1 °C/1 Ma. (For interpretation of the references to colour in this figure legend, the reader is referred to the web version of this article.)

Table 6. Blocking temperatures for cooling rates of optical calcite based on the first-order approximation model of Passey and Henkes (2012) and the pair exchange-diffusion model of Stolper and Eiler (2015) for wet, high-pressure (100 MPa) kinetic parameters from this study, and dry, low-pressure (0.1 MPa) kinetic parameters from Passey and Henkes (2012).

Cooling rate (1 °C per)	Blocking T (°C) first-order approximation		Blocking T (°C) pair exchange-diffusion	
	wet-HP	dry-LP	wet-HP	dry-LP
1 Ma	162	158	145	145
100 ka	179	177	163	165
10 ka	197	196	183	186
1 ka	218	218	205	210
100 years	240	242	229	236
10 years	265	268	255	265
1 year	291	296	284	297
1 month	323	331	318	337
1 day	373	385	372	399
1 h	427	446	429	470
1 min	511	542	518	583
1 s	618	665	627	732

For the pair exchange-diffusion model, we simulated linear cooling from 1000 °C to 0 °C based on the Eqs. (18) and (19) from Stolper and Eiler (2015) adjusted for the wet-HP kinetics of this study and dry-LP kinetics of Passey and Henkes (2012). We modeled blocking temperatures for the same range of cooling rates used in the first-order

approximation model (Fig. 8c and d and Table 6). For rapidly cooling processes, both models predicted a measurable difference in final blocking temperatures between wet-HP and dry-LP conditions. However, at rapid cooling rates the difference in final blocking between wet-HP and dry-LP conditions was larger using the pair exchange-diffusion model compared with the first-order approximation model. For example, the fastest cooling rate of 1 °C/s showed a difference of 105 °C in final blocking temperatures between wet-HP and dry-LP kinetics. The pair exchange-diffusion model predicted lower final blocking temperatures for slow cooling processes, ∼15 °C lower for the slowest cooling rate of 1 °C/Ma, compared with the first-order approximation model (Table 6). Nevertheless, slower cooling regimes had nearly identical blocking temperatures for both wet-HP and dry-LP conditions, similar to findings with the first-order approximation model.

5.3. Water-enhanced diffusivity in calcite

Here we discuss possible implications of our clumped-isotope reordering results for understanding the nature of the "water effect" (*i.e.*, the enhancement of diffusivities in the presence of H_2O relative to dry conditions) observed in previous measurements of calcite C and O diffusivities (Anderson, 1969, Kronenberg et al., 1984, Farver, 1994, Labotka et al., 2000, Labotka et al., 2011). Such diffusivity measurements are generally based on experiments where an external fluid (H_2O, CO_2, or a mixture of these) is labeled with an isotopic tracer (^{13}C, ^{18}O). The mineral/fluid system is heated for some period of time and the propagation of the tracer into the mineral grain (typically ≤1 μm) is later characterized, usually by ion microprobe. In such studies, it is observed that the diffusivity of carbon is largely unaffected by the presence of water (Kronenberg et al., 1984, Labotka et al., 2000), while the diffusivity of oxygen is orders of magnitude greater in wet (H_2O present) conditions compared with dry (CO_2 present, H_2O absent) conditions at pressures of ca. 100 MPa (Kronenberg et al., 1984, Farver, 1994, Labotka et al., 2000, Labotka et al., 2011). However, because these experiments observe only the outer microns of a mineral grain, it is unclear whether this "water effect" only influences the near-surface region, or causes a change in the bulk volume diffusivity of the mineral. Another relevant piece of information is that, under high-pressure conditions, O diffusivity is about three orders of magnitude higher than C diffusivity. Accordingly, under high-pressure, O is significantly more mobile in the calcite lattice than is C, and thus it is not unreasonable to assume that C–O bond reordering at high-pressure is largely a result of O diffusion.

To a first approximation, our observation of minimal change in clumped-isotope reordering rates in wet-HP versus dry-LP conditions suggests that there is little change in the volume diffusivity, since isotopic clumps are distributed throughout the mineral volume, and hence a change in volume diffusivity would be needed to effect a change in clumped-isotope reordering rates. In the temperature range of our experiments (385–450 °C), diffusion coefficients for O diffusion based on tracer diffusion studies are ≥3 orders of magnitude larger in wet conditions compared with dry conditions (Farver, 1994, Labotka et al., 2011), whereas clumped-isotope reordering rate constants are at most 3 *times* higher in wet relative to dry conditions.

For calcite, dissolution of the mineral in water may provide a mechanism for increased diffusivity, creating vacancies at the surface via adsorption of molecular water to the surface and/or dissociated OH^- and H^+ near surface Ca and O, respectively (Kerisit et al., 2005, Lardge et al., 2009, Labotka et al., 2011). One possible mechanism for creating a surface vacancy is a variant on the dissolution reaction:

(13) $2CaCO3+H2O \leftrightarrow 2CaOH++C2O5\square 2-$

where □ represents a vacancy of missing oxygen in one of the carbonate groups on the mineral surface and $CaOH^+$ is coordinated to the mineral surface (Labotka et al., 2011). Such point defects on the crystal face and surface vacancies are possible explanations for the marked increase in O diffusivity for minerals under hydrated conditions. Forward reaction of Eq. (13) or forward reaction followed by surface diffusion would result in a change in $\delta^{18}O$ values, such as observed in this study, but a combination of forward and back reactions could alter the clumped-isotopic composition in the vicinity of the calcite–water interface more than the net change in $\delta^{18}O$ values. Nevertheless, a change in volume diffusivity resulting from such a mechanism would require that the defects generated at the surface are free to diffuse into the volume of the mineral, and are not ‘tied’ to the surface owing to, for example, charge balance considerations.

Another possibility is surface coordination with dissociated water or bonding with associated water can distort the calcite structure in the vicinity of the calcite–water interface (Hochella, 1990b; Lardge et al., 2009, Geissbühler et al., 2004). Such distortion can increase the interatomic spacing at or near the water–calcite interface and increasing potential for interstitial atomic migration (Shewmon, 1963, Hochella, 1990b). Although there is uncertainty about the precise mechanism(s), tracer diffusion studies have firmly established that near-surface O diffusivity increases markedly in the presence of water. However, the question of *extent* remains: is the enhanced O diffusivity limited to the near-surface region (outer few micrometers) that is actually

observed by the tracer propagation/ion microprobe method, or does the enhanced diffusivity extend far into the mineral interior, as a result, for example, of rapid diffusion of water and hydrogen ions (*e.g.*, Farver, 1994; but see Labotka et al., 2011)?

We can explore the volumetric influence of this enhanced diffusivity by modeling the rate constant $k_{ref,obs}$ as follows:

$$k_{ref,obs} = f_{wet}\beta_{wet}k_{ref,dry} + (1-f_{wet})k_{ref,dry} \quad (14)$$

where f_{wet} is the volume fraction of mineral that has water-enhanced kinetics, $k_{ref,dry}$ is the rate constant for dry reaction conditions, and β_{wet} is a multiplicative factor describing increased diffusivity due to the presence of water ($k_{wet} = \beta_{wet}k_{dry}$, where $k_{ref,wet}$ is the rate constant for mineral volume that has been influenced by water). Eq. (14) is independent of geometry but can be applied to a specific geometric form, as shown below. The value for $k_{ref,dry}$ is based on experimental data (Passey and Henkes, 2012). We solve the equation for a range of β_{wet} values. For each β_{wet} value, we solve for the f_{wet} value that reproduces the observed 2.6 ± 0.5 times increase in $k_{ref,obs}$ relative to $k_{ref,dry}$. We can then solve for the penetration depth of enhanced diffusivity l_{wet} by approximating each mineral grain as a perfect cube with edge length l:

$$f_{dry} = 1 - f_{wet} = \frac{V_{dry}}{V_{total}} = \frac{(l-2l_{wet})^3}{l^3} \quad (15)$$

where f_{dry} is the volume fraction of mineral with dry reordering kinetics (*i.e.*, the volume of mineral V_{dry} unaffected by the presence of water), and V_{wet} is the volume of mineral with increased diffusivity due to the presence of water, and V_{total} is the total volume of mineral (*i.e.*, $V_{total} = V_{dry} + V_{wet}$). Our experimental calcite samples have grain sizes ranging from $l = 125$ μm to $l = 250$ μm, and we evaluate l_{wet} for each of these values.

The results are presented in Fig. 9, which shows that penetration depth of increased diffusivity varies inversely with the water-enhanced diffusivity factor β_{wet}. In other words, Fig. 9 shows the combinations of penetration depth and β_{wet} values that are consistent with the observed difference in reordering rate for wet compared to dry conditions. According to this model, if the penetration depth is large, then the water enhancement factor must be small; alternatively, if the water enhancement is large, then the penetration depth must be small in order to explain the modest increase in solid-state reordering rates. The length-scales of O diffusion for our reaction temperatures (0.026–0.006 microns for the longest reaction times (5760 min) at 450 and 385 °C, respectively; see arrows labeled 'x_{mid}' in Fig. 9) predicted by the work of Farver (1994) and Labotka et al. (2000), and is orders of magnitude smaller than the grain sizes examined in our study (125–250 μm). If the mechanisms of C⎯O reordering are largely the same as those for O diffusion, we can seek guidance on appropriate values of β_{wet} using observations for oxygen diffusion coefficients under wet (D_{wet}) and dry (D_{dry})

experimental conditions. Specifically, based on Arrhenius equations for wet O diffusion (Farver, 1994) and dry O diffusion (Labotka et al., 2000), D_{wet}/D_{dry} varies between 0.9×10^3 and 2.8×10^3 for our reaction temperature range of 450–385 °C, respectively. If $\beta_{wet} \approx D_{wet}/D_{dry}$, then inferred penetration depths of water-enhanced diffusivity are similar to mid-distances of diffusion predicted from O diffusion kinetics (Fig. 9). Thus, to the extent that the guidance based on O diffusion is valid for consideration of C–O bond reordering, the inferred penetration depth of enhanced diffusivity is hundredths to tenths of microns.

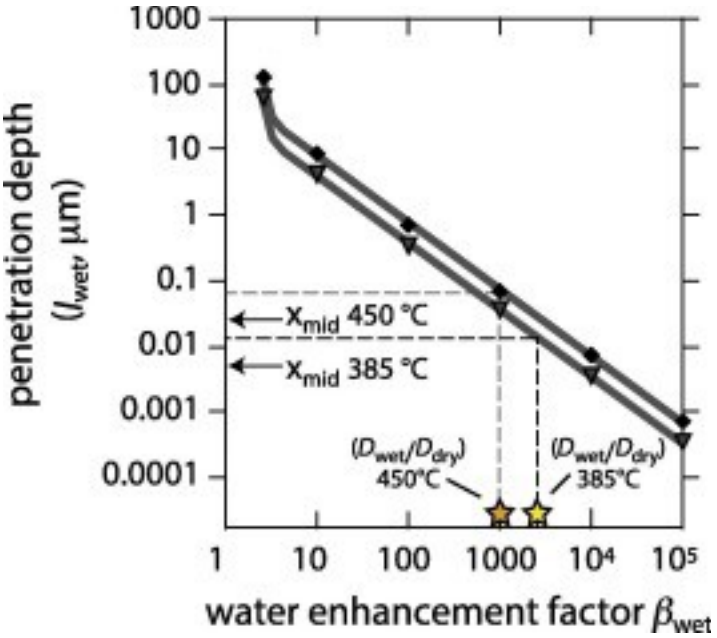

1. Download high-res image (136KB)
2. Download full-size image

Fig. 9. Relationship between modeled penetration depth into the mineral surface of the zone of water-enhanced diffusivity relative to a 'water enhancement factor' describing how wet reordering rate constants relate to dry reordering rate constants. The thick gray lines show the relationship between penetration depth (l_{wet}) of the zone of water-enhanced diffusivity (vertical axis) and water enhancement factor $\beta_{wet} = k_{ref,wet}/k_{ref,dry}$ (see Section for explanation of these parameters). The upper thick gray line marked by diamonds is the solution of Eqs. (14), (15) for 250 mm grains, and the lower thick gray line marked by upside-down triangles is the solution for 125 mm grains. Guidance for the magnitude of the water enhancement factor β_{wet} is provided by the observed ratio of oxygen diffusion coefficients for wet conditions (D_{wet}) and dry conditions (D_{dry}) (orange and yellow stars, respectively). The diffusion coefficients are based on Arrhenius relationships given in Farver (1994) (wet) and Labotka et al. (2000) (dry). The arrows labeled x_{mid} give the mid-distance of oxygen diffusion $(Dt)^{½}$ calculated for wet-HP

conditions in the temperature range of our study (385–450 °C) using the Farver (1994) Arrhenius relation. The inferred penetration depth of the zone of water-enhanced diffusivity (dashed lines) is a small fraction of the total grain size, and is broadly similar to the mid-distance of O diffusion. (For interpretation of the references to colour in this figure legend, the reader is referred to the web version of this article.)

However, the exercise above, and our experimental results in general, speak less to how this zone of water enhanced diffusivity might propagate as a function of time and temperature. Is the zone restricted to the mineral surface owing to surface charge balance considerations, as suggested by Labotka et al. (2011), or can it eventually penetrate deep into the mineral volume? Geological tests of laboratory-derived clumped-isotope reordering kinetics support the former interpretation, since dry reordering kinetics have been generally successful at predicting clumped-isotope compositions of calcites in basin burial and exhumation cycles (*e.g.*, Henkes et al., 2014, Shenton et al., 2015, Lawson et al., in press), and in cooling scenarios such as those resulting from cooling of carbonatites or rapidly exhumed rocks (Dennis and Schrag, 2010, Passey and Henkes, 2012, Stolper and Eiler, 2015). We note that dry kinetic parameters are generally successful at predicting clumped-isotope compositions of geological materials, irrespective of whether the kinetic model of Passey and Henkes (2012) or Stolper and Eiler (2015) is used.

An additional consideration is the role of pressure in the reordering process. A full investigation of the effects of pressure on clumped-isotope bond reordering is beyond the scope of this paper, but here we present ideas that warrant further investigation. Increased pressure generally correlates with decreased diffusivity, for example Ar diffusivity in water-poor rhyolite melts (Behrens and Zhang, 2001) and cation diffusion in garnet (Ganguly, 2010). However, some studies have observed increased diffusivity with increased pressure, for example oxygen diffusivity in dacite melt (Tinker and Lesher, 2001). The increased hydraulic pressure of this study could have altered the calcite structure. SEM images showed twinning planes on reacted calcite crystals that were absent from unreacted crystals (Figs. S1–S6 in Supplementary Material) suggesting the experimental pressure might have caused deformational twinning. Twinning in calcite occurs primarily along the e-plane $\{0\,1\,\bar{1}\,8\}$ (*e.g.*, Ferrill et al., 2004, Rybacki et al., 2013). Such twinning is a change in the crystallographic orientation and bending of the crystal lattice. Nevertheless, it is possible that these structural changes broke discrete bonds within the crystal lattice causing some isotopic bond reordering to occur during twinning. The total increase in reordering rates observed under wet-HP conditions could be a combination of open-system dissolution–

reprecipitation reactions, increased diffusivity in the near-surface environment resulting from water induced surface reactions, and pressure induced structural changes to the calcite crystal lattice. Additional experimentation under dry, high-pressure conditions is needed to investigate the role of pressure in clumped-isotope bond reordering.

6. Conclusions

This study presents the first comparison of calcite clumped-isotope bond reordering kinetics for wet-HP and dry-LP conditions. We observed a small but measureable difference in the rate of change of Δ_{47} values for samples heated under wet-HP conditions compared with dry-LP conditions. Wet-HP samples had consistently lower Δ_{47}values for the same reaction duration compared with dry-LP samples regardless of experimental temperature, except for a single dry-LP duplicate sample, by 0.012–0.069‰. We compared wet-HP and dry-LP reordering kinetics in the context of two different reordering models; the first-order approximation model of Passey and Henkes (2012), and the paired reaction-diffusion model of Stolper and Eiler (2015).

The k_{ref} values for wet-HP conditions were up to ∼3 times greater than dry-LP conditions with the first-order approximation model. The isotope-exchange rate constants (k_f), did not differ between wet-HP and dry-LP conditions with the paired reaction-diffusion model. For the 405 and 425 °C experiments, the diffusion rate constants ($k_{dif\text{-}single}$), and corresponding k_{ref} values for wet-HP conditions of the paired reaction-diffusion model were on average ∼2 times higher than dry-LP conditions, consistent, generally, with the findings of the first-order approximation model. However, the 450 °C experimental data does not differ within error.

We explored temperature–time reordering predictions and rate dependent blocking temperatures based on wet-HP and dry-LP kinetics in the context of the two reordering models. For geologically relevant temperature and time combinations, the difference between wet-HP and dry-LP kinetics was small regardless of model type, but the pair exchange-diffusion model predicted reordering over a broader range of temperature–time combinations compared with the first-order approximation model. Blocking temperatures based on wet-HP and dry-LP kinetics of the first-order approximation model differed by no more than 5 °C for cooling rates from 1 °C/Ma to 1 °C/year and differed by no more than 15 °C based on the pair exchange-diffusion model over the same time period. For fast cooling rates (≥1 °C/year) blocking temperatures were lower for wet-HP conditions than dry-LP conditions, with a difference of 47 °C and 105 °C for the fastest modeled cooling rate of 1 °C/s based on the first-order approximation and pair exchange-diffusion models, respectively.,

Finally, we compared these results to those from traditional oxygen diffusivity studies, which show marked increases in apparent diffusivity (>1000 times at the temperatures of interest to us, ~≤450 °C) when water is present (the “water effect”). We observed only a modest increase on clumped isotope reordering rates (~3 times), which suggests that the water effect does not influence a large fraction of the mineral volume under the temperatures and timescales of our study. In this context, the water effect may be better regarded as surface phenomenon that acts to promote oxygen exchange between mineral and surrounding fluid (Labotka et al., 2011), rather than a change in the oxygen diffusivity of the bulk mineral volume. It is also possible that the increase in reordering rates we observed was not due to the presence of water, but rather to the higher reaction pressure of our experiments compared to earlier ‘dry’ experiments. Future experiments carried out under dry, high pressure conditions could help to evaluate this latter possibility. Regardless, the results of this study suggest that water and pressure have only modest influences on clumped isotope reordering rates. Hence, it appears that meaningful interpretations or predictions can be made of clumped-isotope reordering in calcite, even when the nature and pressure of geological fluids are not precisely known.

Acknowledgments

We thank Michael McCaffery for assistance with SEM imaging and Will Defliese for sharing his clumped-isotope nonlinear mixing model spreadsheet. We also thank Associate Editor Hagit Affek, Theodore Labotka, and two anonymous reviewers for thoughtful comments and suggestions that helped improve the manuscript. This research was funded in part by a grant from the United States National Science Foundation (EAR 1227076) and the American Chemical Society Petroleum Research Fund (PRF 50321-DNI12; PRF 54850-ND2).

Appendix A. Calculated change in calcite $\delta^{18}O$ due to oxygen diffusion

This appendix details our calculation of the change in carbonate $\delta^{18}O$ (VSMOW) values as a result of solid-state diffusion from the mineral–water interface into the interior of the mineral. We assume a simple cube geometry for our 0.250–0.125 mm mesh size samples and use an average cube edge length of 0.1875 mm for all calculations. We calculated the effective distance of O diffusion into the sample as the mid-distance of diffusion according to equation

(A.1)xmid=0.953872(Dt)1/2

where x_{mid} is halfway between the initial concentration C_o and the semi-infinite concentration C_∞, D is the diffusivity of oxygen at a given temperature, and t is the

reaction time (Zhang, 2008). This is the error function solution to diffusion in a semi-infinite medium with constant surface concentration. We used Arrhenius parameters for oxygen self-diffusion reported by Farver (1994) to calculate diffusion coefficients for each experimental temperature.

We then calculated f_{diff}, the fractional volume of the mineral that was influenced by diffusion

(A.2)fdiff=6AxmidVtotal

where A is the surface area of one side of the mineral and V_{total} is the total volume of the mineral. Multiplying by six accounts for the six faces of the mineral. We calculated the isotopic composition of the diffused volume fraction ($\delta^{18}O_{diff}$) by assuming it is in isotopic equilibrium with water (*i.e.*, the −6‰ VSMOW water inside the reaction capsules) at the specific reaction temperature, using equilibrium calcite-water oxygen isotope fractionation factors given by O'Neil et al. (1969). Finally, we calculated the isotopic composition of the bulk mineral using isotopic mass balance:

(A.3)δ18Obulk=fdiffδ18Odiff+(1-fdiff)δ18Oinitial

where $\delta^{18}O_{bulk}$ is the isotopic composition of the bulk mineral after reaction, and $\delta^{18}O_{initial}$ is the composition of mineral before reaction. For reference, the calculated value of x_{mid} for the longest reaction (5740 min) at the highest reaction temperature (450 °C) was 2.6×10^{-8} m, which corresponds to a f_{diff} value of 8.5×10^{-4}, and a change in bulk isotopic composition of reacted calcite ($\delta^{18}O_{bulk}$) of only 0.016‰. Thus solid-state diffusion of O does not account for the ∼0.5‰ change in $\delta^{18}O$ of our reacted samples.

Appendix B. Supplementary material

Download Acrobat PDF file (20MB)Help with pdf files

Supplementary data 1.

Download Word document (125KB)Help with docx files

Supplementary data 2.

References

Affek and Eiler, 2006

H.P. Affek, J.M. Eiler**Abundance of mass 47 CO_2 in urban air, car exhaust, and human breath**
Geochim. Cosmochim. Acta, 70 (2006), pp. 1-12
ArticleDownload PDFView Record in Scopus

Affek et al., 2008

H.P. Affek, M. Bar-Matthews, A. Ayalon, A. Matthews, J.M. Eiler**Glacial/interglacial temperature variations in Soreq cave speleothems as recorded by 'clumped isotope' thermometry**
Geochim. Cosmochim. Acta, 72 (2008), pp. 5351-5360

ArticleDownload PDFView Record in Scopus

Affek and Zaarur, 2014

H.P. Affek, S. Zaarur**Kintic isotope effect in CO_2 degassing: insight from clumped and oxygen isotopes in laboratory precipitation experiments**

Geochim. Cosmochim. Acta, 143 (2014), pp. 319-330

ArticleDownload PDFView Record in Scopus

Anderson, 1969

T.F. Anderson**Self-diffusion of carbon and oxygen in calcite by isotope exchange with carbon dioxide**

J. Geophys. Res., 74 (1969), pp. 3918-3932

CrossRefView Record in Scopus

Beckert et al., 2016

J. Beckert, V. Vandeginste, C.M. John**Exploring the geological features and processes that control the shape and internal fabrics of late diagenetic dolomite bodies (Lower Khuff equivalent – Central Oman Mountains)**

Mar. Pet. Geol., 71 (2016), pp. 1-16

View Record in Scopus

Behrens and Zhang, 2001

H. Behrens, Y. Zhang**Ar diffusion in hydrous silicic melts: implications for volatile diffusion mechanisms and fractionation**

Earth Planet. Sci. Lett., 192 (2001), pp. 363-376

ArticleDownload PDFView Record in Scopus

Bernasconi et al., 2011

S.M. Bernasconi, T.W. Schmid, A.-L. Grauel, J. Mutterlose**Clumped-isotope geochemistry of carbonates: a new tool for the reconstruction of temperature and oxygen isotope composition of seawater**

Appl. Geochem., 26 (2011), pp. S279-S280

ArticleDownload PDFView Record in Scopus

Brown et al., 1999

G.E. Brown Jr., V.E. Henrich, W.H. Casey, D.L. Clark, C.Eggleston, A. Felmy, D.W. Goodman, M. Grätzel, G. Maciel, M.I. McCarthy, K.H. Nealson, D.A. Sverjensky, M.F. Toney, J.M. Zachara**Metal oxide surfaces and their interactions with aqueous solutions and microbial organisms**

Chem. Rev., 99 (1999), pp. 77-174

CrossRefView Record in Scopus

Brown, 2001

G.E. Brown Jr.**How minerals react with water**

Science, 294 (2001), pp. 67-70

CrossRefView Record in Scopus

Came et al., 2007

R.E. Came, J.M. Eiler, J. Veizer, K. Azmy, U. Brand, C.R.Weidman**Coupling of surface temperatures and atmospheric CO_2 concentrations during the Palaeozoic era**
Nature, 449 (2007), pp. 198-201
CrossRefView Record in Scopus

Cummins et al., 2014

R.C. Cummins, S. Finnegan, D.A. Fike, J.M. Eiler, W.W.Fischer**Carbonate clumped isotope constraints on Silurian ocean temperature and seawater $\delta^{18}O$**
Geochim. Cosmochim. Acta, 140 (2014), pp. 241-258
ArticleDownload PDFView Record in Scopus

Daëron et al., 2011

M. Daëron, W. Guo, J. Eiler, D. Genty, D. Blamart, R. Boch, R.Drysdale, R. Maire, K. Wainer, G. Z anchetta**$^{13}C^{18}O$ clumping in speleothems: observations from natural caves and precipitation experiments**
Geochim. Cosmochim. Acta, 75 (2011), pp. 3303-3317
ArticleDownload PDFView Record in Scopus

Daëron et al., 2016

M. Daëron, D. Blamart, M. Peral, H. Affek**Absolute isotopic abundance ratios and the accuracy of Δ_{47}measurements**
Chem. Geol., 441 (2016), pp. 83-96
ArticleDownload PDFView Record in Scopus

Dale et al., 20

1
4

A. Dale, C.M. John, P.S. Mozley, P.C. Smalley, A.H. Muggeridge**Time-capsule concretions: unlocking burial diagenetic processes in the Mancos shale using carbonate clumped isotopes**
Earth Planet. Sci. Lett., 394 (2014), pp. 30-37
ArticleDownload PDFView Record in Scopus

Defliese and Lohmann, 2015

W.F. Defliese, K.C. Lohmann**Non-linear mixing effects on mass-47 CO_2 clumped isotope thermometry: patterns and implications**
Rapid Commun. Mass Spectrom., 29 (2015), pp. 901-909
CrossRefView Record in Scopus

Defliese et al., 2015

W.F. Defliese, M.T. Hren, K.C. Lohmann**Compositional and temperature effects of phosphoric acid fractionation on Δ_{47} analysis and implications for discrepant calibrations**
Chem. Geol., 396 (2015), pp. 51-60
ArticleDownload PDFView Record in Scopus

Dennis and Schr 2010

K.J. Dennis, D.P. Schrag**Clumped isotope thermometry of carbonatites as an indicator of diagenetic alteration**
Geochim. Cosmochim. Acta, 74 (2010), pp. 4110-4122
ArticleDownload PDFView Record in Scopus

Dennis et al., 20

K.J. Dennis, H.P. Affek, B.H. Passey, D.P. Schrag, J.M. Eiler**Defining an absolute reference frame for 'clumped' isotope studies of CO_2**
Geochim. Cosmochim. Acta, 75 (2011), pp. 7117-7131
ArticleDownload PDFView Record in Scopus

Dennis et al., 20

K.J. Dennis, J.K. Cochran, H.H. Landman, D.P. Schrag**The climate of the Late Cretaceous: new insights from the application of the carbonate clumped isotope thermometer to Western Interior Seaway macrofossil**
Earth Planet. Sci. Lett., 362 (2013), pp. 51-65
ArticleDownload PDFView Record in Scopus

Drury and John,

A.J. Drury, C.M. John**Exploring the potential of clumped isotope thermometry on coccolith-rich sediments as a sea surface temperature proxy**
Geochem. Geophys. Geosyst., 17 (2016), pp. 4092-4104
CrossRefView Record in Scopus

Eiler, 2011

J.M. Eiler**Paleoclimate reconstruction using carbonate clumped isotope thermometry**
Quat. Sci. Rev., 30 (2011), pp. 3575-3588
ArticleDownload PDFView Record in Scopus

Farver, 1994

J.R. Farver**Oxygen self-diffusion in calcite: dependence on temperature and water fugacity**
Earth Planet. Sci. Lett., 121 (1994), pp. 575-587
ArticleDownload PDFView Record in Scopus

Ferrill et al., 200

D.A. Ferrill, A.P. Morris, M.A. Evans, M. Burkhard, R.H. GroshongJr., C.M. Onasch**Calcite twin morphology: a low-temperature deformation geothermometer**
J. Struct. Geol., 26 (2004), pp. 1521-1529
ArticleDownload PDFView Record in Scopus

Ferry and Dipple

J.M. Ferry, G.M. Dipple**Fluid flow, mineral reactions, and metasomatism**
Geology, 19 (1991), pp. 211-214
CrossRefView Record in Scopus

Ferry et al., 2011

J.M. Ferry, B.H. Passey, C. Vasconcelos, J.M. Eiler**Formation of dolomite at 40–80 °C in Latemar carbonate buildup, Dolomites, Italy, from clumped isotope thermometry**
Geology, 39 (2011), pp. 571-574
CrossRefView Record in Scopus

Finnegan et al.,

S. Finnegan, K. Bergmann, J.M. Eiler, D.S. Jones, D.A. Fike, I.Eisenman, N.C. Hughes, A.K. Tripati, W.W. Fischer**The magnitude and duration of late Ordovician-early Silurian glaciation**
Science, 331 (2011), pp. 903-906
CrossRefView Record in Scopus

Ganguly, 2010

Ganguly J. (2010) Cation diffusion kinetics in aluminosilicate garnets and geological applications. In Diffusion in Minerals and Melts. (eds. Y. Zhang and D. J. Cherniak). Mineral. Soc. Am., Washington, DC, vol. 72. pp. 559–601.

Geissbühler et a

P. Geissbühler, P. Fenter, E. DiMasi, G. Srajer, L.B.Sorensen, N.C. Sturchio**Three-dimensional structure of the calcite–water interface by surface X-ray scattering**
Surf. Sci., 573 (2004), pp. 191-203

ArticleDownload PDFView Record in Scopus

Ghosh et al., 200

P. Ghosh, J. Adkins, H. Affek, B. Balta, W. Guo, E.A. Schauble, D. Schrag, J.M. Eiler**^{13}C–^{18}O bonds in carbonate minerals: a new kind of paleothermometer**
Geochim. Cosmochim. Acta, 70 (2006), pp. 1439-1456
ArticleDownload PDFView Record in Scopus

Ghosh et al., 200

P. Ghosh, C.N. Garzione, J.M. Eiler**Rapid uplift of the Altiplano revealed through ^{13}C–^{18}O bonds in paleosol carbonates**
Science, 311 (2006), pp. 511-515
CrossRefView Record in Scopus

Gonfiantini et al.

Gonfiantini R., Stichler W. and Rozanski K. (1995) Standards and intercomparison materials distributed by the International Atomic Energy Agency for stable isotope measurements. IAEA-TECDOC-825.

Grauel et al., 201

A.-L. Grauel, T.W. Schmid, B. Hu, C. Bergami, L. Capotondi, L.Zhou, S.M. Bernasconi**Calibration and application of the 'clumped isotope' thermometer to foraminifera for high-resolution climate reconstructions**
Geochim. Cosmochim. Acta, 108 (2013), pp. 125-140
ArticleDownload PDFView Record in Scopus

Henkes et al., 20

G.A. Henkes, B.H. Passey, E.L. Grossman, B.J. Shenton, A.Pérez-Huerta, T.E. Yance y**Temperature limits for preservation of primary calcite clumped isotope paleotemperatures**
Geochim. Cosmochim. Acta, 139 (2014), pp. 362-382
ArticleDownload PDFView Record in Scopus

Hier-Majumder e

S. Hier-Majumder, I.M. Anderson, D.L. Dohlstedt**Influence of protons on Fe-Mg interdiffusion in olivine**
J. Geophys. Res., 110 (2005), p. B02202

Hill et al., 2014

P.S. Hill, A.K. Tripati, E.A. Schauble**Theoretical constraints on the effects of pH, salinity, and temperature on clumped isotope signatures of dissolved inorganic carbon species and precipitating carbonate minerals**
Geochim. Cosmochim. Acta, 125 (2014), pp. 610-652
ArticleDownload PDFView Record in Scopus

Hochella and Wh

Hochella M. F. Jr. and White A. F. (1990a) Mineral–water interface geochemistry: an overview. In Mineral–Water Interface Geochemistry (eds. M. F. Hochella Jr. and A. G. White). Mineral. Soc. Am., Washington, DC, vol. 23. pp. 1–15.

Hochella, 1990b

Hochella M. F. Jr. (1990b) Atomic structure, microtopography, composition, and reactivity of mineral surfaces. In Mineral–Water Interface Geochemistry (eds. M. F. Hochella Jr. and A. G. White). Mineral. Soc. Am., Washington, DC, vol. 23. pp. 87–132.

Huntington et al.

K.W. Huntington, J.M. Eiler, H.P. Affek, W. Guo, M. Bonifacie, L.Y. Yeung, N. Thiagarajan, B. Passey, A. Tripati, M. Daëron, R. Came**Methods and limitations of 'clumped' CO_2 isotope (Δ_{47}) analysis by gas-source isotope ratio mass spectrometry**
J. Mass Spectrom., 44 (2009), pp. 1318-1329
CrossRefView Record in Scopus

Huntington et al.

K.W. Huntington, B.P. Wernicke, J.M. Eiler**Influence of climate change and uplift on Colorado Plateau paleotemperatures from carbonate clumped isotope thermometry**
Tectonics, 29 (2010), pp. 1-19
View Record in Scopus

Huntington et al.

K.W. Huntington, J. Saylor, J. Quade, A.M. Hudson**High late Miocene-Pliocene elevation of the Zhada basin, southwestern Tibetan plateau, from carbonate clumped isotope thermometry**
Geol. Soc. Am. Bull., 127 (2014), pp. 181-199
View Record in Scopus

Huntington and L

K.W. Huntington, A.R. Lechler**Carbonate clumped isotope thermometery in continental tectonics**
Tectonophysics, 647–648 (2015), pp. 1-20
ArticleDownload PDFView Record in Scopus

Kar et al., 2016

N. Kar, C.N. Garzione, C. Jaramillo, T. Shanahan, V. Carlotto, A.Pullen, F. Moreno, V. Anderson, E. Moreno, J. Eiler**Rapid regional surface uplift of the northern Altiplano plateau revealed by multiproxy paleoclimates reconstruction**
Earth Planet. Sci. Lett., 447 (2016), pp. 33-47
ArticleDownload PDFView Record in Scopus

Kerisit et al., 200

S. Kerisit, A. Marmier, S.C. Parker**Ab initio surface phase diagram of the {10$\bar{1}$4} calcite surface**
J. Phys. Chem. B, 109 (2005), pp. 18211-18213
CrossRefView Record in Scopus

Kluge et al., 201

T. Kluge, H.P. Affek, Y.G. Zhang, Y. Dublyansky, C. Spötl, A.Immenhauser, D.K. Richter**Clumped isotope thermometry of cryogenic cave carbonates**

Geochim. Cosmochim. Acta, 126 (2014), pp. 541-554

ArticleDownload PDFView Record in Scopus

Kronenberg et al

A.K. Kronenberg, R.A. Yund, B.J. Giletti**Carbon and oxygen diffusion in calcite: effects of Mn content and P_{H2O}**

Phys. Chem. Miner., 11 (1984), pp. 101-112

CrossRefView Record in Scopus

Labotka et al., 2

T.C. Labotka, D.R. Cole, L.R. Riciputi**Diffusion of C and O in calcite at 100 MPa**

Am. Miner., 85 (2000), pp. 488-494

CrossRefView Record in Scopus

Labotka et al., 2004

T.C. Labotka, D.R. Cole, L.R. Riciputi, M. Fayek**Diffusion of C and O in calcite from 0.1 to 200 MPa**

Am. Miner., 89 (2004), pp. 799-806

CrossRefView Record in Scopus

Labotka et al., 2011

T.C. Labotka, D.R. Cole, M.T. Fayek, T. Chacoko**An experimental study of the diffusion of C and O in calcite in mixed CO_2–H_2O fluids**

Am. Miner., 96 (2011), pp. 1262-1269

CrossRefView Record in Scopus

Lardge et al., 2009

J.S. Lardge, D.M. Duffy, M.J. Gillan**Investigation of the interaction of water with the calcite (10.4) surface using ab initio simulation**

J. Phys. Chem. C, 113 (2009), pp. 7207-7212

CrossRefView Record in Scopus

Lawson et al., in press

Lawson M., Shenton B. J., Stolper D. A., Eiler J. M., Rasbury E. T., Becker T. P., Phillips-Lander C. M., Buono A. S., Becker S. P., Pottorf R., Gray G. G., Yurewicz D. and Gournay J. (in press) Deciphering the diagenetic history of the El Abra Formation of eastern Mexico using reordered clumped isotope temperatures and U-Pb dating. Geol. Soc. Am. Bull. http://doi.org/10.1130/B31656.1.

Leier et al., 2013

A. Leier, N. McQuarrie, C. Garzione, J. Eiler**Stable isotope evidence for multiple pulses of rapid surface uplift in the Central Andes, Bolivia**

Earth Planet. Sci. Lett., 371–372 (2013), pp. 49-58

ArticleDownload PDFView Record in Scopus

Li et al., 2015

S. Li, N.E. Levin, L.A. Chesson**Continental scale variation in ^{17}O-excess of meteoric waters in the United States**

Geochim. Cosmochim. Acta, 164 (2015), pp. 110-126

ArticleDownload PDFView Record in Scopus

Lloyd et al., 2017

M.K. Lloyd, J.M. Eiler, P.I. Nabelek**Clumped isotope thermometry of calcite and dolomite in a contact metamorphic environment**

Geochim. Cosmochim. Acta, 197 (2017), pp. 323-344

ArticleDownload PDFView Record in Scopus

O'Neil et al., 1969

J.R. O'Neil, R.N. Clayton, T.K. Mayeda**Oxygen isotope fractionation in divalent metal carbonates**

J. Chem. Phys., 51 (1969), pp. 5547-5558

CrossRefView Record in Scopus

Passey et al., 2010

B.H. Passey, N.E. Levin, T.E. Cerling, F.H. Brown, J.M. Eiler**High-temperature environments of human evolution in East Africa based on bond ordering in paleosol carbonates**

Proc. Natl. Acad. Sci., 107 (2010), pp. 11245-11249

CrossRefView Record in Scopus

Passey and Henkes, 2012

B.H. Passey, G.A. Henkes**Carbonate clumped isotope bond reordering and geospeedometry**

Earth Planet. Sci. Lett., 351–352 (2012), pp. 223-236

ArticleDownload PDFView Record in Scopus

Quade et al., 2011

J. Quade, D.O. Breecker, M. Daëron, J. Eiler**The paleoaltimetry of Tibet: an isotopic perspective**

Am. J. Sci., 311 (2011), pp. 77-115

CrossRefView Record in Scopus

Ryb et al., 2017

U. Ryb, M.K. Lloyd, D.A. Stolper, J.M. Eiler**The clumped-isotope geochemistry of exhumed marbles from Naxos, Greece**

Earth Planet. Sci. Lett., 470 (2017), pp. 1-12

ArticleDownload PDFView Record in Scopus

Rybacki et al., 2013

E. Rybacki, B. Evans, C. Janssen, R. Wirth, G. Dresen**Influence of stress, temperature, and strain on calcite twins constrained by deformation experiments**

Techonophysics, 601 (2013), pp. 20-36

ArticleDownload PDFView Record in Scopus

Saenger et al., 2012

C. Saenger, H.P. Affek, T. Felis, N. Thiagarajan, J.M. Lough, M.Holcomb**Carbonate clumped isotope variability in shallow water corals: temperature dependence and growth-related vital effects**

Geochim. Cosmochim. Acta, 99 (2012), pp. 224-242

ArticleDownload PDFView Record in Scopus

Schauble et al., 2006

E.A. Schauble, P. Ghosh, J.M. Eiler**Preferential formation of $^{13}C–^{18}O$ bonds in carbonate minerals, estimated using first-principles lattice dynamics**

Geochim. Cosmochim. Acta, 70 (2006), pp. 2510-2529

ArticleDownload PDFView Record in Scopus

Schauer et al., 2016

A.J. Schauer, J. Kelson, C. Saenger, K.W. Huntington**Choice of ^{17}O correction affects clumped isotope (Δ_{47}) values of CO_2measured with mass spectrometry**

Rapid Comm. Mass Spectrom., 30 (2016), pp. 2607-2616

CrossRefView Record in Scopus

Shenton et al., 2015

B.J. Shenton, E.L. Grossman, B.H. Passey, G.A. Henkes, T.P.Becker, J.C. Laya, A. Perez-Huerta, S.P. Becker, M. Lawson**Clumped isotope thermometry in deeply buried sedimentary carbonates: the effects of bond reordering and recrystallization**

Geol. Soc. Am. Bull., 127 (7–8) (2015), pp. 1036-1051

View Record in Scopus

Shewmon, 1963

P.G. Shewmon**Diffusion in Solids**

McGraw-Hill Book Company, New York (1963)

Siman-tov et al., 2016

S. Siman-tov, H.P. Affek, A. Matthews, E. Aharonov, Z.Reches**Shear heating and clumped isotope reordering in carbonate faults**

Earth Planet. Sci. Lett., 445 (2016), pp. 136-145

ArticleDownload PDFView Record in Scopus

Stolper and Eiler, 2015

D.A. Stolper, J.M. Eiler**The kinetics of solid-state isotope-exchange reactions for clumped isotopes: a study of inorganic calcites and apatites from natural and experimental samples**

Am. J. Sci., 315 (2015), pp. 363-411

CrossRefView Record in Scopus

Tinker and Lesher, 2001

D. Tinker, C.E. Lesher**Self diffusion of Si and O in dacitic liquid at high pressures**

Am. Miner., 86 (2001), pp. 1-13

CrossRefView Record in Scopus

Tripati et al., 2015

A.K. Tripati, P.S. Hill, R.A. Eagle, J.L. Mosenfelder, J. Tang, E.A.Schauble, J.M. Eiler, R.E. Zeebe, J. Uchikawa, T.B. Coplen, J.B. Ries, D.Henry**Beyond temperature: clumped isotope signatures in dissolved inorganic carbon species and the influence of solution chemistry on carbonate mineral composition**

Geochim. Cosmochim. Acta, 166 (2015), pp. 34-371

Wang et al., 2004

Z. Wang, T. Hiraga, D.L. Kohlstedt**Effect of H+ on Fe-Mg interdiffusion in olivine, (Fe, Mg)$_2$SiO$_4$**

Appl. Phys. Lett., 85 (2004), pp. 209-211

CrossRefView Record in Scopus

Zhang, 2008

Y. Zhang**Geochemical Kinetics**

Princeton Univ. Press, New Jersey (2008)

[1]

Present address: Department of Earth and Environmental Sciences, University of Michigan, Ann Arbor, MI 48109, USA.

$$\mathrm{Ca^{13}C^{18}O^{16}O_2} + \mathrm{Ca^{12}C^{16}O_3} \leftrightarrow \mathrm{Ca^{13}C^{16}O_3} + \mathrm{Ca^{12}C^{18}O^{16}O_2} \quad (1)$$

$$\Delta_{47} = \left[\left(\frac{R^{47}}{R^{*47}} - 1\right) - \left(\frac{R^{46}}{R^{*46}} - 1\right) - \left(\frac{R^{45}}{R^{*45}} - 1\right)\right] \times 1000 \quad (2)$$

$$\Delta_{47}^{meas} = f_{precip}\Delta_{47}^{precip} + (1 - f_{precip})\Delta_{47}^{corrected} \quad (3)$$

$$\ln\left[\frac{\Delta_{47}^{t}-\Delta_{47}^{eq}}{\Delta_{47}^{init}-\Delta_{47}^{eq}}\right]=\ln\left[1-\frac{\Delta_{47}^{init}-\Delta_{47}^{t}}{\Delta_{47}^{init}-\Delta_{47}^{eq}}\right]=\ln[1-F]=-kt \quad (4)$$

where

$$F=\frac{\Delta_{47}^{init}-\Delta_{47}^{t}}{\Delta_{47}^{init}-\Delta_{47}^{eq}} \quad (5)$$

and Δ_{47}^{init} is the initial value of the sample, Δ_{47}^{t} is the value of the sample at a given temperature *T* for a period of time *t*, Δ_{47}^{eq} is the theoretical value for a sample in equilibrium at a given temperature *T*, and *k* is the reaction rate. Equilibrium Δ_{47} values as a function of temperature were calculated according to Eq. (5) of Passey and Henkes (2012). Linear fits to the first-order reaction progress for each temperature yield slopes that correspond to *k* at that temperature (Fig. 3b). The slope of a linear regression of ln(*k*) versus 1/*T* from the various experiments yields the activation energy, E_a, and the y-intercept is ln(k_o). The Arrhenius equation is:

$$k=k_o\exp\left(\frac{-E_a}{RT}\right) \quad (6)$$

where *k* is the reaction progress rate constant, *R* is the gas constant, and *T* is the temperature in kelvins (Fig. 3c). This is equivalent to

$$k=k_{ref}\exp\left(\frac{E_a}{R}\left(\frac{1}{T_{ref}}-\frac{1}{T}\right)\right) \quad (7)$$

$$^{12}\mathrm{C}^{16}\mathrm{O}_3^{2-} + {}^{12}\mathrm{C}^{16}\mathrm{O}_2{}^{18}\mathrm{O}^{2-} \leftrightarrow \mathrm{pair} \tag{8}$$

and

$$\mathrm{pair} \leftrightarrow {}^{13}\mathrm{C}^{16}\mathrm{O}_{3,\,single}^{2-} + {}^{12}\mathrm{C}^{16}\mathrm{O}_2{}^{18}\mathrm{O}_{single}^{2-} \tag{9}$$

where pair refers to adjacent $^{12}\mathrm{C}^{16}\mathrm{O}_3^{2-}$ and $^{12}\mathrm{C}^{16}\mathrm{O}_2{}^{18}\mathrm{O}^{2-}$ groups and single refers to a species with single isotopic substitution that does not have another singly isotopically substituted species in an adjacent location in the crystal lattice. Reaction progress in the paired reaction-diffusion model is described by the following equations (Stolper and Eiler, 2015):

$$\frac{d\xi}{dt} = k_f\left(\left[{}^{12}\mathrm{C}^{16}\mathrm{O}_3^{2-}\right]_\mathrm{o}\right)\left(\left[{}^{13}\mathrm{C}^{16}\mathrm{O}_2{}^{18}\mathrm{O}^{2-}\right]_\mathrm{o} - \xi\right) - k_b[\mathrm{pair}]_t \tag{10}$$

and

$$\begin{aligned}\frac{d\mathrm{pair}}{dt} &= k_f\left(\left[{}^{12}\mathrm{C}^{16}\mathrm{O}_3^{2-}\right]_\mathrm{o}\right)\left(\left[{}^{13}\mathrm{C}^{16}\mathrm{O}_2{}^{18}\mathrm{O}^{2-}\right]_\mathrm{o} - \xi\right) - k_b[\mathrm{pair}]_t \\ &+ k_{dif-single}\left[{}^{12}\mathrm{C}^{16}\mathrm{O}_2{}^{18}\mathrm{O}^{2-}\right]_{single,\mathrm{o}}\left[{}^{13}\mathrm{C}^{16}\mathrm{O}_3^{2-}\right]_{single,\mathrm{o}} \\ &- k_{dif-pair}[\mathrm{pair}]_t\end{aligned} \tag{11}$$

$$\begin{aligned}\Delta_{47}^{i} &= (\Delta_{47}^{i-1} - \Delta_{47}^{eq,i})\exp\left\{-\Delta t k_{ref}\exp\left[\frac{E_a}{R}\right]\left(\frac{1}{T_{ref}} - \frac{1}{T}\right)\right\} \\ &+ \Delta_{47}^{eq,i}\end{aligned} \tag{12}$$

$$2\mathrm{CaCO_3} + \mathrm{H_2O} \leftrightarrow 2\mathrm{CaOH^+} + \mathrm{C_2O_5}\square^{2-} \tag{13}$$

$$\mathrm{k}_{\mathrm{ref,obs}} = f_{\mathrm{wet}}\beta_{\mathrm{wet}}k_{\mathrm{ref,dry}} + (1 - f_{\mathrm{wet}})k_{\mathrm{ref,dry}} \quad (14)$$

where f_{wet} is the volume fraction of mineral that has water-enhanced kinetics, $k_{ref,dry}$ is the rate constant for dry reaction conditions, and β_{wet} is a multiplicative factor describing increased diffusivity due to the presence of water ($k_{wet} = \beta_{wet}k_{dry}$, where $k_{ref,wet}$ is the rate constant for mineral volume that has been influenced by water). Eq. (14) is independent of geometry but can be applied to a specific geometric form, as shown below. The value for $k_{ref,dry}$ is based on experimental data (Passey and Henkes, 2012). We solve the equation for a range of β_{wet} values. For each β_{wet} value, we solve for the f_{wet} value that reproduces the observed 2.6 ± 0.5 times increase in $k_{ref,obs}$ relative to $k_{ref,dry}$. We can then solve for the penetration depth of enhanced diffusivity l_{wet} by approximating each mineral grain as a perfect cube with edge length l:

$$f_{\mathrm{dry}} = 1 - f_{\mathrm{wet}} = \frac{V_{\mathrm{dry}}}{V_{\mathrm{total}}} = \frac{(l-2l_{\mathrm{wet}})^3}{l^3} \quad (15)$$

$$x_{mid} = 0.953872(Dt)^{1/2} \quad \text{(A.1)}$$

where x_{mid} is halfway between the initial concentration C_o and the semi-infinite concentration C_∞, D is the diffusivity of oxygen at a given temperature, and t is the reaction time (Zhang, 2008). This is the error function solution to diffusion in a semi-infinite medium with constant surface concentration. We used Arrhenius parameters for oxygen self-diffusion reported by Farver (1994) to calculate diffusion coefficients for each experimental temperature.

We then calculated f_{diff}, the fractional volume of the mineral that was influenced by diffusion

$$f_{diff} = \frac{6Ax_{mid}}{V_{total}} \quad \text{(A.2)}$$

where A is the surface area of one side of the mineral and V_{total} is the total volume of the mineral. Multiplying by six accounts for the six faces of the mineral. We calculated the isotopic composition of the diffused volume fraction ($\delta^{18}O_{diff}$) by assuming it is in isotopic equilibrium with water (*i.e.*, the −6‰ VSMOW water inside the reaction capsules) at the specific reaction temperature, using equilibrium calcite-water oxygen isotope fractionation factors given by O'Neil et al. (1969). Finally, we calculated the isotopic composition of the bulk mineral using isotopic mass balance:

$$\delta^{18}\mathrm{O}_{\mathrm{bulk}} = f_{diff}\delta^{18}\mathrm{O}_{\mathrm{diff}} + (1 - f_{diff})\delta^{18}\mathrm{O}_{\mathrm{initial}} \quad \text{(A.3)}$$